3-28-2014

DNA-Functionalized Gold Nanoparticles for Chemiresistive Vapor Sensing

Kan Fu
University of Connecticut - Storrs, kan.fu@uconn.edu

DNA-Functionalized Gold Nanoparticles for Chemiresistive Vapor Sensing

Kan Fu

B. Eng., National University of Singapore, 2011

A thesis submitted to the faculty of the University of the Connecticut in partial fulfillment of the requirements for the degree of Master of Science

University of Connecticut

2014

APPROVAL PAGE

Masters of Science Thesis

DNA-Functionalized Gold Nanoparticles for Chemiresistive Vapor Sensing

Presented by

Kan Fu, B. Eng.

Major Advisor _____
Brian G. Willis

Associate Advisor _____
Bryan D. Huey

Associate Advisor _____
Yu Lei

University of Connecticut

2014

ACKNOWLEDGMENTS

Reflecting on my over two years of time at University of Connecticut, I feel very thankful to the great people I have met and the valuable opportunities I have had. While my first project after I finished my college degree has been lined with challenges and hardships, I have always felt blessed and spirited.

First and foremost, many thanks to my advisor, Dr. Brian G. Willis, for his invaluable guidance, patience, trust, vision, encouragement and support in my work. Also, to my team mates, Han Wang, Xiaoqiang Jiang, and Jie Qi, for always lending a helping hand and providing me with endless moral support.

Thanks to Dr. Yong Wang and Shihui Li from the Pennsylvania State University for a very pleasant and close collaboration on this project. Thanks to Dr. Yu Lei and Dr. Bryan D. Huey for providing lab space and equipment for this project and for serving on my advisory committee. Thanks Dr Lichun Zhang and Dr Roger Ristau for assistance in electron microscopy, and many thanks to Nathanael Chan, Andrew LaMarche, and Wyatt Pedrick for their diligent undergraduate research work.

My friends both in the village of Storrs and across the three continents around the world have given me immense practical and emotional support, to whom I extend my heartfelt gratitude. Thanks to my wonderful roommates, my buddies, friends and colleagues in Singapore, UK, China and USA for your help and being concerned about me.

Finally, all my love to my parents and my extended family in China, for always being there for me. Your everlasting support inspires me to move forward.

TABLE OF CONTENTS

LIST OF FIGURES

LIST OF TABLES

ABSTRACT

Chemiresistive sensing with functionalized gold nanoparticles is a powerful new technology for vapor sensing. Utilizing changes in behavior of electron tunneling through conductive gold nanoparticles and insulating organic capping layers upon analyte adsorption, this system can achieve intrinsically high sensitivity and rapid response time. A number of thiol-based small-molecule organic ligands have already been successfully used to functionalize gold nanoparticles, yielding an array of organic sensors having various sensitivities towards different organic vapors. With the aid of chemometric analysis tools, gold nanoparticle-based chemiresistive sensors have been rapidly maturing into a vapor quantification and identification technology.

A limiting factor for its success, as has been the case for many types of sensors based on reversible physical adsorption, is the lack of specific interaction between sensor material and the vapor analytes. Therefore, the vapor identification capability is limited. A method to overcome this, using DNA-functionalized gold nanoparticles, is proposed in this study. Although highly specific molecular recognition is not yet achievable, this preliminary reveals many characteristics of DNA-functionalized gold nanoparticle for sensing purpose. Using non-specially designed DNA sequences, gold nanoparticle sensors display similar kinds of swelling-dominated response behavior with sequence-dependent response patterns towards organic vapors. Due to the polyelectrolyte nature of DNA molecules, the sensors behave specially towards water vapor, displaying a dichotomous behavior. At low relative humidities, the sensors are swelling-

dominated, showing an increase in sensor response with increasing relative humidity. At medium to high relative humidities, the sensors are ionic-conduction dominated, showing a rapid decrease in resistivity by a few orders of magnitude with increasing relative humidity. Sensor responses towards organic vapor analytes are mediated by environmental relative humidity, with both a response sign switch and response enhancement observed. The chemiresistive effects of DNA-functionalized nanoparticles were also influenced by the DNA chain length, with higher response exhibited by longer DNA chain length. However, the response magnitude normalized by chain length is approximately constant. Lastly, the sequence-dependence behavior is explored by using two DNA molecules of identical composition but different nucleobase sequences. A comparison with alkanethiol-functionalized gold nanoparticles indicates that the sensors respond by swelling behavior under dry conditions, but possibly conformational-dependent response is present. The findings in this preliminary but comprehensive study of DNA-functionalized gold nanoparticles suggest the potential future developments of highly selective and highly diverse chemiresistive sensors for specific vapor analytes.

Chapter 1

INTRODUCTION

1.1 Vapor sensors

Vapor sensing is a rapidly evolving technology. Fast, sensitive, and accurate detection of volatile organic compounds (VOCs) in gaseous samples is one of the central goals of modern analytical chemistry, with potential applications in the future bound to transform the way of life and improve our standard of living. For example, vapor sensing is necessary for monitoring of hazardous VOC emissions in a workplace environment, for detecting leaks along chemical pipelines and storage tanks, for revealing explosive and radioactive compounds in public areas, for checking food safety, as well as for diagnosing diseases and providing early warning of potential health problems [1]. Theoretically, successful analysis of vapor analytes can be universally performed with gas chromatography-mass spectrometry (GC-MS) instrumentation, allowing both accurate identification and quantification in the parts-per-trillion range [2]. However, high cost, bulkiness, lengthy analytical process, labor-intensiveness, as well as a highly skilled workforce required to operate it, prohibit the practical wide deployment of GC-MS for field applications. Developing portable, low-cost, low-power, durable, and easy-to-operate sensors represents the most viable solution to the problem.

Sensors are small analytical devices in which a sensing material either is applied onto a suitable physical transducer or simultaneously also serves as a transducer to convert a change in a property of the sensing material into a readable signal. Current knowledge and understanding

of the nature have enabled a variety of transduction mechanisms to be explored. For example, surface acoustic wave (SAW) sensors [3], quartz-crystal microbalance (QCM) sensors [4], fiber-optic vapor sensors [5], fluorescence quenching sensors [6], microelectromechanical systems (MEMS) sensors [7], surface-enhanced Raman scattering (SERS) sensors [8], chemiresistive sensors [9], chemicapacitive sensors [10], field effect chemitransistor (ChemFET) sensors [11], and inductively coupled RFID sensors [12].

Across all these fields, scientists and engineers are actively trying to improve the sensors' sensitivity and vapor identification capabilities to match those of a commercial GC-MS, with varying degrees of success. In many cases, the limit of detection (LOD) of sensors can achieve or go beyond those of commercial GC-MS. Notably, Fido® explosive detector series, based on amplifying fluorescence polymers (AFP), is capable of detecting 1 part per quadrillion of trinitrotoluene (TNT) [13]. In another report, pristine graphene chemiresistors achieved sensitivity on the order of 100 parts per quadrillion for small-molecule gases [14]. As far as sensitivity is concerned, achieving GC-MS performance is relatively easy. However, as sensors work unequivocally on an adsorption-desorption phenomenon with many VOCs share similar properties, a common limitation to all these sensor concepts is the lack of satisfactory vapor identification capability. With no column-based separation process preluding vapor detection, cross-sensitivity towards different vapors and interference from background fluctuations would cause inaccurate quantification, inaccurate determination of desired compounds [15], or worse, giving false signals. Therefore a parallel goal to achieving sensitivity, but of a more challenging nature, is to attain vapor identification capability. The adoption of sensor arrays and chemometric analysis using statistical tools such as principal component analysis (PCA) and linear discriminant analysis (LDA) is of great value to improve the vapor identification

capabilities. Statistical analysis gains confidence through a large number of samples and a large sensor array of different sensing materials. Therefore, vapor identification capability could be enhanced through designing a more diverse array of sensors. Still, a large enough sensor array is insufficient to generate the highly specific ligand-receptor type of binding phenomena typically seen in biological sensors. For example, commercial glucose sensors which depend on enzymatic breakdown of glucose by glucose oxidase [16], and under-development aptamer-based sensors for specific detection of thrombin [17]. To match vapor sensors with the highly specific detection mechanism displayed by aqueous-based biological sensor system remains a formidable challenge.

1.2 Chemiresistive Vapor Sensors

The simplest, probably also the most versatile type of all above-mentioned sensors is the chemiresistive sensor. A schematic of a simple chemiresistive sensor is pictured in Figure 1.1. The sensor is typically excited through application of an AC or DC potential across the two electrodes, and the current through the sensor is monitored. Upon reversible adsorption of vapor analytes into the responsive film which is typically made of polymers, metal oxides, semi-metal oxides, or composites, the resistance of the film changes and is then recorded. Sensor response depends on the conduction mechanism within the sensor material and also depends on adsorption properties of vapor phase analytes into this thin film sensor material.

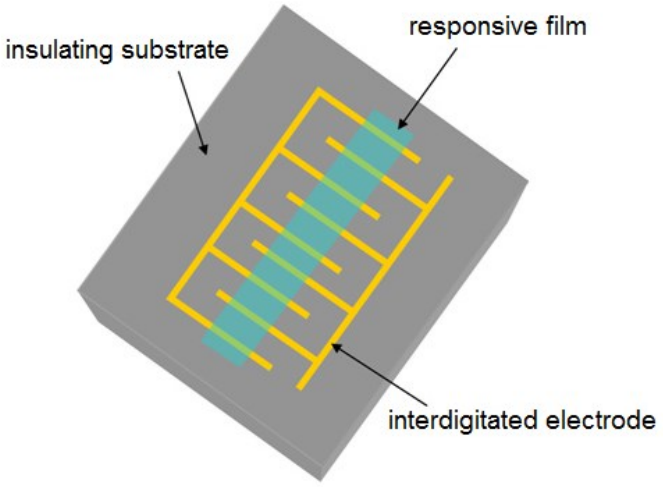

Figure 1.1 Schematic of a chemiresistive sensor comprised of interdigitated electrodes (in gold) covered with a film of a responsive material

Chemiresistive sensors have several advantages over other type of sensors. First, owing to the simple voltage-current transduction mechanism, chemiresistive sensors can be cheaply made and interfaced with network-scale management and read-out circuitry for remote management and multi-dimensional data collection. This allows easy construction of sensor networks [18] for monitoring environments as small as a storage room and as large as a global climate monitoring systems. Second, the thin film structure of chemiresistive sensors makes it compatible with standard microfabrication and nanofabrication technology, allowing sensor integration and miniaturization. Third, as the transducer portion of the sensor is virtually independent of the sensing material, material substitution is relatively easy. A huge number of material candidates can be used, potentially creating a gigantic array of sensors which improves the vapor identification confidence.

1.2.1 Nanogaps as Sensing Devices

Nanogaps are finely separated metal electrodes with a gap in the range of 1 – 2 nm where electrons can tunnel through. They are the basic component of molecular electronic devices, which are lauded as a promising approach to move beyond traditional device scaling to develop future nanoelectronic technologies. Nanogap could either have an empty space in between the gap to form an open gap, or with some molecules placed in the middle of the nanogap serving specific purposes. For example, it allows the studies of electron transport through single molecules [19], and it also provides a platform of using the intrinsic properties of molecules for important applications [20]. Figure 1.2 shows a schematic diagram of a multiple-substituted aromatic ring molecule placed in between a nanogap to be used as the building block for a molecular transistor.

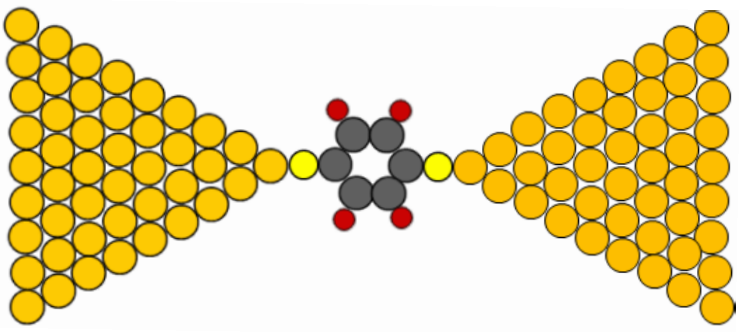

Figure 1.2 Schematics of a single-molecule transistor

One important application of nanogap devices is in sensing. Due to differences in electronic transport properties through the nanogap devices when the inserted molecules are different, sensitivity to different molecular species could be easily measured through monitoring the electronic conductivity through the nanogaps when a bias is applied. Through electrical

measurements, nanogaps have been shown to be useful for hydrogen sensing [21], ultrasensitive detection of solution-phase DNA [22], and vapor sensing [23]. The use of nanogaps represents the way of achieving the smallest-scale chemiresistive vapor sensing device sensors. Nanogap chemiresistive sensors have several advantages over traditional bulk material sensors. First, being small in volume, it is saturated much faster and reaches vapor adsorption equilibrium status faster than bulk materials. Second, as only a small current needs to pass through the sensor, power consumption is greatly reduced. In fact, ideal nanogap sensors drawing nanoamperes (nA) of current, is an excellent candidate for self-powered sensor networks running on energy harnessed from the environment using existing technology. Third, although the building cost of the sensor platform may be high, sensing material cost is saved especially when the cost of sensing material is high. However, engineering single nanogaps remains a challenge, mainly due to difficulties in controlling single-molecule geometry within the nanogap, molecular conformation, binding site or metal-molecule interface, and electrode orientation [24]. Therefore, the realization of mature and reproducible nanogap sensors needs sub-nanometer precision in process control – a technology yet to be developed. Fortunately, current research has been able to fabricate devices that integrate an ensemble of tunnel junctions through a combination of bottom-up and top-down approaches.

1.2.2 Gold Nanoparticle Chemiresistive Vapor Sensors

Gold nanoparticles are an important tool to build nanogap sensors using available technologies. While utilizing identical chemiresistive sensor setup and circuitry, gold nanoparticles functionalized with a layer of organic moieties are used as a composite material to replace the conducting polymer or metal oxide film traditionally used in chemiresistive sensors. Functionalized gold nanoparticles are usually synthesized by reducing a gold ion precursor in the

presence of organic ligands. Depending on the desired final product, the as-synthesized gold nanoparticles are then further subject to ligand exchange process to produce a variety of surface functionalities. Well-studied ligands are unfunctionalized alkanethiols, with chain length from six carbons to twelve carbons [25], as well as amino-[26], phenyl-[27], carboxyl-, and hydroxyl-[28] functionalized alkanethiols. To fabricate the sensor devices, a solution of functionalized gold nanoparticle solutions is typically drop-casted [29], airbrushed [25], ink-jetted [30], or dip-coated [31] onto a microfabricated interdigitated electrode on a substrate. The solution drop is then dried to form the nanoparticle composite film. Figure 1.3 shows some gold nanoparticle chemiresistive sensor devices of varying geometry.

As a composite material consisting of a highly conductive phase and an insulating phase, the resistance of gold nanoparticle chemiresistor film is in the semiconductor range. Electronic conduction is through an electron hopping mechanism through a chain of conducting gold nanoparticles which form a path. Electron-transport mechanism between the electrode and gold nanoparticle cores is the same as that between gold nanoparticle cores. Therefore contact resistance, which would have been a complicating issue in traditional chemiresistors, would be essentially avoided [32]. This fact lends help to further miniaturization of sensors, because contact contribution to the electron transport would be small even if only a few gold nanoparticles were present. Electron transport is affected by the media they need to pass through when it hops from one nanoparticle to the next. Figuratively, the gold nanoparticle film is an array of nanogaps, and its response arises from the collective functioning of a multitude of nanogap sensors.

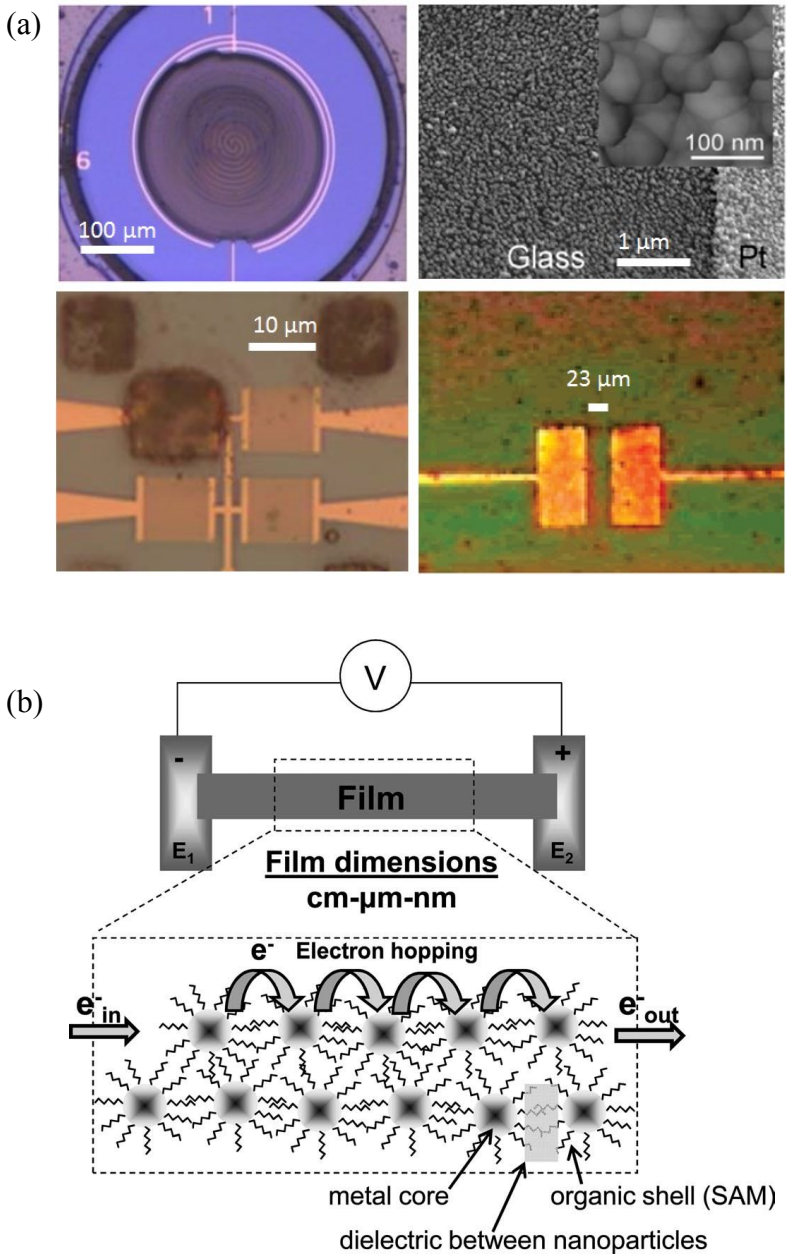

Figure 1.3 (a) Various types of gold nanoparticle chemiresistive sensors [31, 33-35] (b) Schematic representation of a chemiresistive film of various dimensions comprised of metal monolayer-protected clusters (MPCs) separated by interdigitated SAM molecules [36]

As vapor phase molecules reversibly adsorb and dissolve into the gold nanoparticle films, swelling of the films occurs, and film resistance changes following the relationship

$$R = \exp(\beta l)\exp\left(-\frac{E_c}{k_B T}\right) \tag{1.1}$$

where β is a decay constant related to the probability of interparticle electron tunneling, l is the interparticle distance, E_c is the activation energy, and k_B is the Boltzmann constant. Further, the activation energy is given by

$$E_c = \frac{1}{4\pi\varepsilon_0\varepsilon_r}\frac{e^2}{r} \tag{1.2}$$

where e is the fundamental charge, ε_0 is the vacuum permittivity, ε_r is the dielectric constant of the organic capping layer separating nanoparticles, and r is the radius of the gold nanoparticle. It has already been established that both the interparticle distance and the dielectric constant of organic capping layer affect sensor response strongly [37-38], and these two factors are ultimately determined by the intrinsic polarity [28, 37] and molecular size [39-40] of capping layer molecules. However, it has not been well-established which effect – distance change or dielectric constant change – is the dominant factor in resistivity change of the nanocomposite film.

When an array of gold nanoparticle chemiresistive vapor sensors with different surface functionalities are used in parallel, varying degrees of response to the same vapor arise from different sensors due to difference in partition coefficients of a certain vapor molecule into different surface organic layers. "Electronic noses" are sensor arrays whose output signals are

further processed by pattern recognition algorithms or neural network hardware. They are powerful systems to classify, identify, and where necessary quantify, vapors or odors of concern [41]. Functionalized gold nanoparticles are an enhancing addition to the family of electronic noses because of the large library of surface ligands to choose from, sensor stability, as well as the advantages mentioned earlier. Sensor arrays based on gold nanoparticle nanocomposite films have been used for breath analysis in cancer screening [29] and pollutant analysis in sea water [30], and general volatile organic vapors in air [42]. With the help chemometric equipment, the sensor arrays can perform analyses such as differentiating two mixtures of different compositions, or identify some components in a mixture of compounds. With their small size, fast response time, sensitivity and limits of detection (LOD) matching the state-of-the-art vapor sensors to date, gold nanoparticle chemiresistive vapor sensors are rapidly maturing. Despite this success, one of the remaining challenges for gold nanoparticle chemiresistive sensors, as mentioned in Section 1.1 earlier for all current vapor sensor technologies, is still the lack of selectivity. The selectivity of functionalized gold nanoparticles towards a pair vapors of similar molecular weights, for example toluene and hexane, can rarely reach a factor of 10 [15, 28]. Chemometric statistical tools might allow an array of sensors to differentiate some vapors from others. However, confidence in chemometric tools depends on the array size. Currently, the number of useful ligands for gold nanoparticle functionalization is less than 30 [15, 29, 36]. With limited number of different small molecule nanoparticle ligands available but many vapors to be differentiated, the vapor differentiation and identification capability of gold nanoparticle electronic noses needs to be further improved.

1.3 Biomolecules as Vapor Sensing Elements

Selectivity engineering for vapor sensors is widely regarded as an immense challenge. Current selective vapor sensors depend hugely on a specific chemical or physical transduction mechanism. For example, the most mature humidity (water vapor) sensors utilize either ionic currents or electric double layer capacitance activated by condensed water [43]. Hydrogen sensors are usually heavily dependent on selective adsorption of hydrogen gas on palladium to from a hydride [44]. Phosgene sensors work primarily on the selective reaction of phosgene with amines to produce hydrochloric acid, thus inducing ionic conduction [45]. These sensors are highly reliable and selective, with interference from environmental atmosphere rarely a concern. However, these highly selective sensors acquired their selectivity from specific analyte-sensor interactions, which are very limited in types and numbers. Many sensor systems are more inclined to be group-sensitive. They are sensitive towards a group of similar compounds with little distinguishing power between different member compounds of the same family. For example, grapheme oxide optical sensors differentiate vapors based on hydrophilicity and hydrophobicity of vapors [46]. Fluorescence quenching properties of nitroaromatic compounds were used to generate selectivity of amplifying fluorescence polymers (AFP) towards nitroaromatic compounds. The selectivity over non-nitroaromatic compounds, such as toluene, is as large as 10 times. The notable selectivity towards nitroaromatic compounds led to the commercial deployment of this technology as Fido® series explosives detector in military use [47].

As seen from the above examples, vapor selectivity could be either individual or group-based, depending on the nature of transduction mechanism. The selectivity is governed hugely by known specific physical or chemical interactions. For an arbitrary compound of interest, if a

selective transduction mechanism cannot be found, an individual or group-selective sensor would be non-existent.

1.3.1 Sensor Selectivity

Arguably, one of the most sophisticated features of chemistry in biological systems is molecular recognition mechanism. Highly selective recognition and reaction mechanisms, with multiple reactions and signaling pathways occurring simultaneously within a physiological environment, are the key to a stable functioning living system. As opposed to the various specific transduction mechanisms discussed above, biological selectivity is purely thermodynamic. For an associative process involving an analyte (A) and the receptor molecule (R), the binding event to form an analyte-receptor complex (C) is simply

$$\mathrm{A} + \mathrm{R} \leftrightarrow \mathrm{C} \tag{1.3}$$

And the association and dissociation constants representing the forward and reverse reactions are respectively

$$K_a = \frac{[\mathrm{C}]}{[\mathrm{A}][\mathrm{R}]} \tag{1.4}$$

$$K_d = \frac{[\mathrm{A}][\mathrm{R}]}{[\mathrm{C}]} \tag{1.5}$$

Previously mentioned small-molecule organothiol functionalized gold nanoparticles can be understood by a similarly purely thermodynamic principle. In non-biological materials, the adsorption of vapors into the solid phase is typically quantified using the partition coefficient, K_e.

$$K_e = \frac{C_s}{C_v} \tag{1.6}$$

where C_s is the concentration of the analyte in the solid phase and C_v is the concentration of the analyte in the vapor phase. Although bearing different physical meaning than the ligand-receptor equilibrium, valid comparisons can be made within each individual system to show selectivity. For biological sensors, selectivity comparison can be made by comparing K_a or K_d values for an individual analyte or a group of vapor analytes. While for non-biological materials, K_e values are usually compared. It needs to be noted that the selectivities discussed here are purely materials-based, and their incorporation into transducers would possibly alter the selectivity differences. Nevertheless, when sensor transducers are identical for both biological and non-biological materials, the selectivity differences are powerful representations of the analyte distinguishing capabilities of these two classes of sensors.

1.3.2 Non-specific Organic Materials and Selectivity

The study by Patrash et. al. gave a comprehensive comparison of vapor analyte selectivity on four types of common polymer coatings were compared using a simple surface acoustic wave (SAW) transducer. SAW transducer reveals K_e values more accurately than gold nanoparticles as the signal changes result primarily from mass changes by adsorption with relatively less effect from the material property changes such as modulus changes [48]. A total of 39 vapors were tested on four materials – poly[bis(cyanoallyl)-siloxane], poly(methylphenylsiloxane), poly(phenyl ether) and poly(isobutylene). Other than being polymeric in structure, the materials are of similar chemical properties to the organic coatings on gold nanoparticle sensors discussed in Section 1.2.1 in terms of functional groups and polarity.

SAW sensors work primarily through the vapor partitioning mechanism, and is non-specific. The K_e values for sensing different vapors were summarized in Patrash's study, and it is clearly visible that for vapors of similar structures, the K_e values are close. For example, K_e (toluene) / K_e (benzene) values assume a value of 2 – 3, while K_e (2-propanol)/ K_e (methanol) values are in the range of 1 – 3. These values point to two limitations of simple organic materials as the sensor materials. First, the selectivity against each specific vapor pair is very low, and second, the differences in selectivity values (K_e ratios) are also very small. For a different vapor pair such as toluene and hexane, K_e (toluene) / K_e (hexane) values improved to 4 – 25. This larger difference is mainly due to structural differences between the vapor analytes. Though of similar molecular weights, toluene more readily partition into the organic phases. However, there are many vapors such as benzene and butanone sharing similar K_e with toluene and many vapors such as isooctane and ethyl ether sharing similar K_e with hexane, therefore these vapors could easily interfere with the measurement vapors of interest.

1.3.3 Biological Selectivity

To improve sensor selectivity, engineers have long sought to building bio-inspired molecular recognition systems to improve sensing systems. In liquid-based systems, extensive success has been achieved. A classic example is the enzymatic glucose sensor. The selective element in question – glucose oxidase, is 270 to 600 times more selective towards glucose than other common reducing sugars xylose, galactose, and mannose [49]. In addition to protein-based sensors, aptamer-based sensors have also exhibited to high specificity. An example, shown in Figure 1.4, is the single strand DNA (ss-DNA)-based oxytetracycline sensors which display at least hundreds of times of selectivity over structural analogues tetracycline and doxycycline [50]. The K_d values of the selected aptamers towards oxytetracycline were in the range 9 – 57 nM,

while K_d values of these aptamers towards tetracycline and doxycycline are in the μM range or too large to be measured. They were reported not to bind at all to some aptamers [50]. Compared with non-specific organic materials discussed in section 1.3.2, the advantage of aptamers to distinguish between molecules with closely resembling structures is conspicuous. Other DNA aptamers were also designed for selective detection of small molecule targets including cocaine, ATP [51] , and trinitrotoluene (TNT) [52]. The capability of biomolecule-based sensors to differentiate structurally similar molecules is immense.

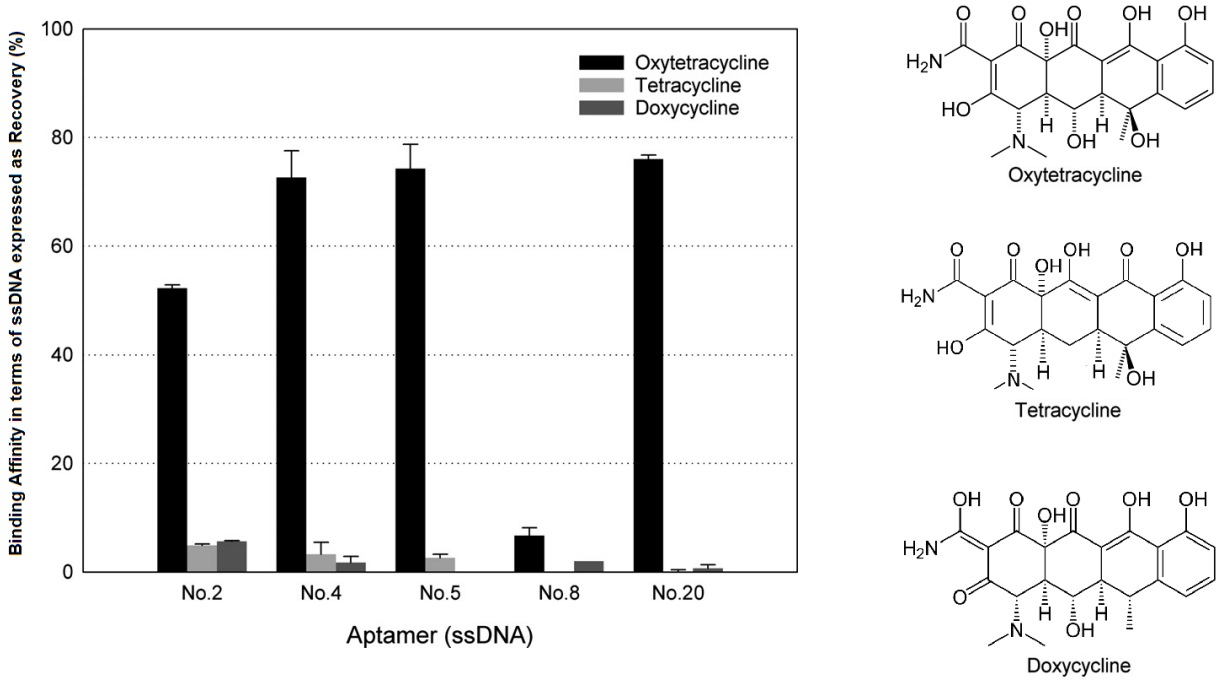

Figure 1.4 Binding affinities of five aptamers to structural similar targets. One microgram of each ssDNA was incubated with constant number of beads coated with equimolar concentrations of oxytetracycline, tetracycline, and doxycycline. Aptamers bound to the target-coated beads were eluted by heat treatment, and binding affinity is expressed as concentration of eluted ssDNA calculated as percentage of DNA recovery. [50]

1.3.4 Use of DNA in Vapor Sensors

Biomolecule selectivity in aqueous phase inspires adaptation of the same type of molecules for vapor sensing. A potential solution that may enable enhanced specificity is to incorporate nucleic acid oligomers as molecular recognition elements for gas phase sensing. The interest in nucleic acid oligomers over proteins is their higher stability. More importantly, a large number of base sequences can be created. The number of possible unique receptor configurations scales with the length N of the oligomer as 4^N, giving rise to a large diversity of sensing elements. In addition, DNA oligomers may be used to develop aptamers, which are short oligonucleotides that bind target analytes with high specificity.

As oligomeric nucleotide sequences for selective sensing are most commonly used in solution, no reports have shown their selective behavior in vapor phase. Therefore, DNA for vapor sensing, though challenging, could potentially open up a new exciting field that revolutionize the sensors industry. Recent reports have included fluorescence-based solid-state sensors that respond to target vapor analytes through sorption-induced changes of fluorescence intensity. White et al. used 29 different ss-DNA sequences tagged with dye molecules to create sensor arrays, and measured their response to volatile compounds. Sensors were made by simply depositing the dye-labeled DNA films on glass substrates and fluorescence response towards vapor exposure was measured, producing diverse response patterns. The number of distinct sequences employed was roughly twice as many as other gold nanoparticle-based chemiresistive sensor arrays reported to date [53]. Others have proposed modifying nucleobases with fluorescent groups to give fluorescence responses to organic vapors [54].

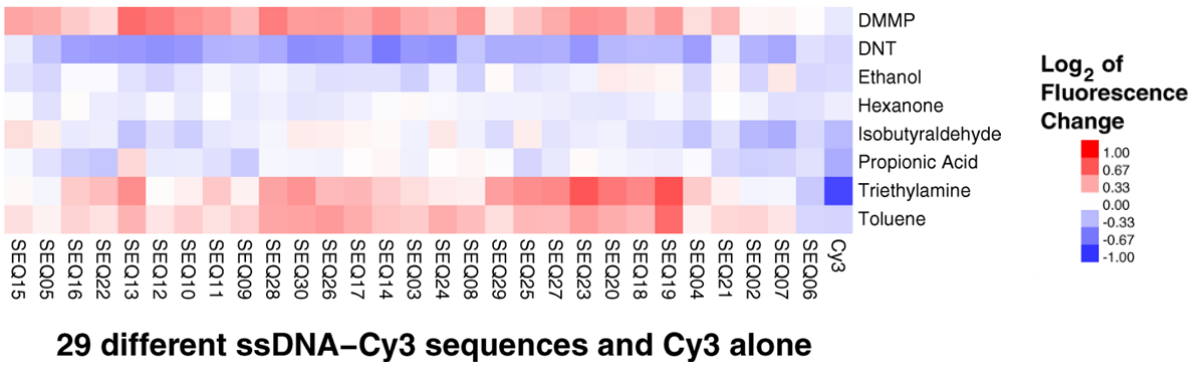

Figure 1.5 Fluorescence responses of 29 distinctive Cy3-labeled ssDNA sequences towards a set of 8 vapors [53]

Beside fluorescence-based sensors, semiconductor devices have also been reported. Polynucleotides have also been used to functionalize chemitransistors made from carbon nanotubes (CNT) [55-56] and graphene [57]. The use of carbon nanotubes and graphene is also very close to the theme of molecular electronics. These studies demonstrate the potential for sequence-dependent chemical recognition capability with DNA oligomers in the vapor phase.

1.4 Research Goals

The objectives of this research program are to investigate DNA-functionalized gold nanoparticles as a new material for chemiresistive vapor sensors. The concept of DNA-functionalized gold nanoparticles for chemiresistive vapor sensing originates from the integration of the high-performing nanogap chemiresistive sensors and possibly enhanced selectivity offered by DNA functionalization. A new technology thus interfacing solid state devices and biological behavior is aspired.

To produce DNA-functionalized gold nanoparticles suitable for chemiresistive vapor sensors, a method compatible with aqueous ligand exchange needs to be developed. In this study, a technique using citrate-stabilized gold nanoparticles as a starting material was investigated [58]. The material for deposition was first characterized to show DNA binding to the surface, both in aqueous condition and in as-deposited dry nanocomposite condition.

Electrical measurements were then carried out to test the electronic transport properties of DNA gold nanoparticle chemiresistive sensors under vapor sensing conditions. To start the experiment, interdigitated electrodes with similar dimensions to those in literature to simplify the device fabrication processes were used. Using similar electrode designs also allows a direct comparison between DNA-functionalized gold nanoparticle sensors and organothiol-functionalized nanoparticle sensors. A special sensor evaluation chamber was constructed, and sensors were exposed to common volatile organic vapors and their responses were compared. The sensing performances in terms of sensitivity and selectivity of DNA-functionalized gold nanoparticle sensors were directly compared with organothiol-functionalized gold nanoparticles. In addition, the sensors were studied to understand the effect of chain length and sequence differences on sensor response patterns.

A significant challenge for DNA-based vapor sensing is to extend their function from solution-based to solid-state devices. Water interacts strongly with DNA, altering the microscopic structures of both double-stranded [59-60] and single-stranded DNA [60] molecules so that sensitivity to water may be expected in solid-state devices. Many prior studies of chemiresistor devices have used relatively hydrophobic sensing materials that are not particularly sensitive to humidity [61-62], but there are at least a few examples where sensitivity to water

vapor has been observed [63]. Control of humidity effects in solid state DNA-based sensing has been considered in some studies [53, 56], but the effect of water on chemiresistive vapor sensing has not been systematically studied. As DNA is a highly polar molecule with ionized phosphate groups and multiple hydration shells [64-65], it is anticipated that humidity may have a significant effect on DNA-based absorptive sensors. It is therefore imperative to measure the effects of humidity on such materials. To show the effect of relative humidity on DNA gold nanoparticle vapor sensors, the sensors were exposed to organic vapors for testing in the presence of water vapor. The difference in conduction mechanisms were also explored through impedance spectroscopy.

1.5 References

1. Potyrailo, R. A.; Mirsky, V. M. Combinatorial and High-Throughput Development of Sensing Materials: The First 10 Years. *Chemical Reviews* **2008,** *108* (2), 770-813.

2. Settle, F. A. *Handbook of instrumental techniques for analytical chemistry*; Prentice Hall PTR 1997.

3. Wohltjen, H. Mechanism of operation and design considerations for surface acoustic wave device vapour sensors. *Sensors and Actuators* **1984,** *5* (4), 307-325.

4. Du, X.; Wang, Z.; Huang, J.; Tao, S.; Tang, X.; Jiang, Y. A new polysiloxane coating on QCM sensor for DMMP vapor detection. *J Mater Sci* **2009,** *44* (21), 5872-5876.

5. Barnard, S. M.; Walt, D. R. Fiber-optic organic vapor sensor. *Environmental Science & Technology* **1991,** *25* (7), 1301-1304.

6. Thomas, S. W.; Joly, G. D.; Swager, T. M. Chemical Sensors Based on Amplifying Fluorescent Conjugated Polymers. *Chemical Reviews* **2007,** *107* (4), 1339-1386.

7. Lang, H.; Hegner, M.; Gerber, C. Nanomechanical Cantilever Array Sensors. In *Springer Handbook of Nanotechnology*, Bhushan, B., Ed.; Springer Berlin Heidelberg, 2007, pp 443-460.

8. Tamane, S.; Topal, C. O.; Kalkan, A. K. In *Vapor phase SERS sensor for explosives detection*, Nanotechnology (IEEE-NANO), 2011 11th IEEE Conference on, 15-18 Aug. 2011; 2011, pp 301-306.

9. Franke, M. E.; Koplin, T. J.; Simon, U. Metal and Metal Oxide Nanoparticles in Chemiresistors: Does the Nanoscale Matter? *Small* **2006,** *2* (1), 36-50.

10. Patel, S. V.; Mlsna, T. E.; Fruhberger, B.; Klaassen, E.; Cemalovic, S.; Baselt, D. R. Chemicapacitive microsensors for volatile organic compound detection. *Sensors and Actuators B: Chemical* **2003,** *96* (3), 541-553.

11. Lazzerini, G. M.; Strambini, L. M.; Barillaro, G. Addressing Reliability and Degradation of Chemitransistor Sensors by Electrical Tuning of the Sensitivity. *Sci. Rep.* **2013,** *3*.

12. Potyrailo, R. A.; Burns, A.; Nagraj, N.; Surman, C.; Morris, W.; Zhexiong, T.; Lee, D. J.; McGinniss, E.; Forster, I.; Watkins, H.; Farrell, J. In *Multivariable passive RFID vapor sensors: Pilot-scale manufacturing and laboratory evaluation*, Future of Instrumentation International Workshop (FIIW), 2011, 7-8 Nov. 2011; 2011, pp 32-33.

13. Woodfin, R. L. *Trace Chemical Sensing of Explosives*; Wiley 2006.

14. Chen, G.; Paronyan, T. M.; Harutyunyan, A. R. Sub-ppt gas detection with pristine graphene. *Applied Physics Letters* **2012,** *101* (5), -.

15. Steinecker, W. H.; Rowe, M. P.; Zellers, E. T. Model of Vapor-Induced Resistivity Changes in Gold−Thiolate Monolayer-Protected Nanoparticle Sensor Films. *Analytical Chemistry* **2007,** *79* (13), 4977-4986.

16. Oliver, N. S.; Toumazou, C.; Cass, A. E. G.; Johnston, D. G. Glucose sensors: a review of current and emerging technology. *Diabetic Medicine* **2009,** *26* (3), 197-210.

17. So, H.-M.; Won, K.; Kim, Y. H.; Kim, B.-K.; Ryu, B. H.; Na, P. S.; Kim, H.; Lee, J.-O. Single-Walled Carbon Nanotube Biosensors Using Aptamers as Molecular Recognition Elements. *Journal of the American Chemical Society* **2005,** *127* (34), 11906-11907.

18. Akyildiz, I. F.; Weilian, S.; Sankarasubramaniam, Y.; Cayirci, E. A survey on sensor networks. *Communications Magazine, IEEE* **2002,** *40* (8), 102-114.

19. Kumar, A.; Heimbuch, R.; Poelsema, B.; Zandvliet, H. J. W. Controlled transport through a single molecule. *Journal of Physics: Condensed Matter* **2012,** *24* (8), 082201.

20. Sergey, K.; Andrey, D.; Mattias, H.; Jérôme, C.; Jean-Luc, B.; Nicolai, S.-H.; Per, H.; Thomas, B. Single-electron transistor of a single organic molecule with access to several redox states. *Nature* **2003,** *425* (6959), 698-701.

21. Lee, J.; Shim, W.; Noh, J.-S.; Lee, W. Design Rules for Nanogap-Based Hydrogen Gas Sensors. *ChemPhysChem* **2012,** *13* (6), 1395-1403.

22. Roy, S.; Chen, X.; Li, M.-H.; Peng, Y.; Anariba, F.; Gao, Z. Mass-Produced Nanogap Sensor Arrays for Ultrasensitive Detection of DNA. *Journal of the American Chemical Society* **2009,** *131* (34), 12211-12217.

23. Gupta, R.; Appelbaum, I.; Willis, B. G. Reversible Molecular Adsorption and Detection Using Inelastic Electron Tunneling Spectroscopy in Monolithic Nanoscopic Tunnel Junctions. *The Journal of Physical Chemistry C* **2009,** *113* (9), 3874-3880.

24. Hsu, I. J. Characterization of ALD Copper Thin Films on Palladium Seed Layers for Molecular Electronics. Ph.D Thesis, University of Delaware 2008.

25. Wohltjen, H.; Snow, A. W. Colloidal Metal−Insulator−Metal Ensemble Chemiresistor Sensor. *Analytical Chemistry* **1998,** *70* (14), 2856-2859.

26. Krasteva, N.; Besnard, I.; Guse, B.; Bauer, R. E.; Müllen, K.; Yasuda, A.; Vossmeyer, T. Self-Assembled Gold Nanoparticle/Dendrimer Composite Films for Vapor Sensing Applications. *Nano Letters* **2002,** *2* (5), 551-555.

27. Kim, Y. J.; Pyo, H.-B.; Park, S.-H. In *Response Properties of the Gold Nanoparticle Sensors toward Benzene and Toluene Vapors*, Sensors, 2006. 5th IEEE Conference on, 22-25 Oct. 2006; 2006, pp 1078-1080.

28. Evans, S. D.; Johnson, S. R.; Cheng, Y. L.; Shen, T. Vapour sensing using hybrid organic-inorganic nanostructured materials. *Journal of Materials Chemistry* **2000,** *10* (1), 183-188.

29. Peng, G.; Tisch, U.; Adams, O.; Hakim, M.; Shehada, N.; Broza, Y. Y.; Billan, S.; Abdah-Bortnyak, R.; Kuten, A.; Haick, H. Diagnosing lung cancer in exhaled breath using gold nanoparticles. *Nat Nano* **2009,** *4* (10), 669-673.

30. Cooper, J. S.; Raguse, B.; Chow, E.; Hubble, L.; Müller, K.-H.; Wieczorek, L. Gold Nanoparticle Chemiresistor Sensor Array that Differentiates between Hydrocarbon Fuels Dissolved in Artificial Seawater. *Analytical Chemistry* **2010,** *82* (9), 3788-3795.

31. Tokonami, S.; Shiigi, H.; Nagaoka, T. Preparation of Nanogapped Gold Nanoparticle Array for DNA Detection. *Electroanalysis* **2008,** *20* (4), 355-360.

32. Ancona, M. G.; Snow, A. W.; Foos, E. E.; Kruppa, W.; Bass, R. Scaling Properties of Gold Nanocluster Chemiresistor Sensors. *Sensors Journal, IEEE* **2006,** *6* (6), 1403-1414.

33. Niti, G.; Ashok, M.; Nathan, L.; Lawrence, S.; Tony, R. R.; Suresh, S.; Lee, W.; Jay, L. S.; Gary, K. F.; Rongchao, J. Robust gold nanoparticles stabilized by trithiol for application in chemiresistive sensors. *Nanotechnology* **2010,** *21* (40), 405501.

34. Covington, E.; Bohrer, F. I.; Xu, C.; Zellers, E. T.; Kurdak, C. Densely integrated array of chemiresistor vapor sensors with electron-beam patterned monolayer-protected gold nanoparticle interface films. *Lab on a Chip* **2010,** *10* (22), 3058-3060.

35. Ibañez, F. J.; Zamborini, F. P. Reactivity of Hydrogen with Solid-State Films of Alkylamine- and Tetraoctylammonium Bromide-Stabilized Pd, PdAg, and PdAu Nanoparticles

for Sensing and Catalysis Applications. *Journal of the American Chemical Society* **2007,** *130* (2), 622-633.

36. Ibañez, F. J.; Zamborini, F. P. Chemiresistive Sensing with Chemically Modified Metal and Alloy Nanoparticles. *Small* **2012,** *8* (2), 174-202.

37. Ibañez, F. J.; Zamborini, F. P. Chemiresistive Sensing of Volatile Organic Compounds with Films of Surfactant-Stabilized Gold and Gold−Silver Alloy Nanoparticles. *ACS Nano* **2008,** *2* (8), 1543-1552.

38. Joseph, Y.; Guse, B.; Vossmeyer, T.; Yasuda, A. Gold Nanoparticle/Organic Networks as Chemiresistor Coatings: The Effect of Film Morphology on Vapor Sensitivity. *The Journal of Physical Chemistry C* **2008,** *112* (32), 12507-12514.

39. Snow, A. W.; Ancona, M. G.; Park, D. Nanodimensionally Driven Analyte Response Reversal in Gold Nanocluster Chemiresistor Sensing. *Langmuir* **2012,** *28* (44), 15438-15443.

40. Joseph, Y.; Besnard, I.; Rosenberger, M.; Guse, B.; Nothofer, H.-G.; Wessels, J. M.; Wild, U.; Knop-Gericke, A.; Su, D.; Schlögl, R.; Yasuda, A.; Vossmeyer, T. Self-Assembled Gold Nanoparticle/Alkanedithiol Films: Preparation, Electron Microscopy, XPS-Analysis, Charge Transport, and Vapor-Sensing Properties†. *The Journal of Physical Chemistry B* **2003,** *107* (30), 7406-7413.

41. Lewis, N. S. Electronic Nose. http://nsl.caltech.edu/research:nose.

42. García-Berríos, E.; Gao, T.; Theriot, J. C.; Woodka, M. D.; Brunschwig, B. S.; Lewis, N. S. Response and Discrimination Performance of Arrays of Organothiol-Capped Au Nanoparticle Chemiresistive Vapor Sensors. *The Journal of Physical Chemistry C* **2011,** *115* (14), 6208-6217.

43. Chen, Z.; Lu, C. Humidity sensors: a review of materials and mechanisms. *Sensor Letters* **2005,** *3* (4), 274-295.

44. Foster, C. Hydrogen sensors are faster, more sensitive. http://www.innovations-report.com/html/reports/physics_astronomy/report-44815.html.

45. Virji, S.; Kojima, R.; Fowler, J.; Villanueva, J.; Kaner, R.; Weiller, B. Polyaniline nanofiber composites with amines: Novel materials for phosgene detection. *Nano Res.* **2009,** *2* (2), 135-142.

46. Some, S.; Xu, Y.; Kim, Y.; Yoon, Y.; Qin, H.; Kulkarni, A.; Kim, T.; Lee, H. Highly Sensitive and Selective Gas Sensor Using Hydrophilic and Hydrophobic Graphenes. *Sci. Rep.* **2013,** *3*.

47. FLIR. Fido NXT Next Generation Explosive Detection. http://http://gs.flir.com/products/icx-detection/explosives/fido-nxt/.

48. Patrash, S. J.; Zellers, E. T. Characterization of polymeric surface acoustic wave sensor coatings and semiempirical models of sensor responses to organic vapors. *Analytical Chemistry* **1993,** *65* (15), 2055-2066.

49. Adams Jr, E. C.; Mast, R. L.; Free, A. H. Specificity of glucose oxidase. *Archives of Biochemistry and Biophysics* **1960,** *91* (2), 230-234.

50. Niazi, J. H.; Lee, S. J.; Kim, Y. S.; Gu, M. B. ssDNA aptamers that selectively bind oxytetracycline. *Bioorganic & Medicinal Chemistry* **2008,** *16* (3), 1254-1261.

51. Lee, J.-O.; So, H.-M.; Jeon, E.-K.; Chang, H.; Won, K.; Kim, Y. Aptamers as molecular recognition elements for electrical nanobiosensors. *Anal Bioanal Chem* **2008,** *390* (4), 1023-1032.

52. Ehrentreich-Förster, E.; Orgel, D.; Krause-Griep, A.; Cech, B.; Erdmann, V.; Bier, F.; Scheller, F. W.; Rimmele, M. Biosensor-based on-site explosives detection using aptamers as recognition elements. *Anal Bioanal Chem* **2008,** *391* (5), 1793-1800.

53. White, J.; Truesdell, K.; Williams, L. B.; AtKisson, M. S.; Kauer, J. S. Solid-State, Dye-Labeled DNA Detects Volatile Compounds in the Vapor Phase. *PLoS Biol* **2008,** *6* (1), e9.

54. Samain, F.; Ghosh, S.; Teo, Y. N.; Kool, E. T. Polyfluorophores on a DNA Backbone: Sensors of Small Molecules in the Vapor Phase. *Angewandte Chemie International Edition* **2010,** *49* (39), 7025-7029.

55. Staii, C.; Johnson, A. T.; Chen, M.; Gelperin, A. DNA-Decorated Carbon Nanotubes for Chemical Sensing. *Nano Letters* **2005,** *5* (9), 1774-1778.

56. Kybert, N. J.; Lerner, M. B.; Yodh, J. S.; Preti, G.; Johnson, A. T. C. Differentiation of Complex Vapor Mixtures Using Versatile DNA–Carbon Nanotube Chemical Sensor Arrays. *ACS Nano* **2013,** *7* (3), 2800-2807.

57. Lu, Y.; Goldsmith, B. R.; Kybert, N. J.; Johnson, A. T. C. DNA-decorated graphene chemical sensors. *Applied Physics Letters* **2010,** *97* (8), 083107.

58. Liu, J.; Lu, Y. Preparation of aptamer-linked gold nanoparticle purple aggregates for colorimetric sensing of analytes. *Nat. Protocols* **2006,** *1* (1), 246-252.

59. Fuller, W.; Forsyth, T.; Mahendrasingam, A. Water–DNA interactions as studied by X–ray and neutron fibre diffraction. *Philosophical Transactions of the Royal Society of London. Series B: Biological Sciences* **2004,** *359* (1448), 1237-1248.

60. Hanczyc, P.; Åkerman, B.; Nordén, B. Short Oligonucleotides Aligned in Stretched Humid Matrix: Secondary DNA Structure in Poly(vinyl alcohol) Environment. *Langmuir* **2012,** *28* (16), 6662-6669.

61. Zilberman, Y.; Ionescu, R.; Feng, X.; Müllen, K.; Haick, H. Nanoarray of Polycyclic Aromatic Hydrocarbons and Carbon Nanotubes for Accurate and Predictive Detection in Real-World Environmental Humidity. *ACS Nano* **2011,** *5* (8), 6743-6753.

62. Bayn, A.; Feng, X.; Müllen, K.; Haick, H. Field Effect Transistors Based on Polycyclic Aromatic Hydrocarbons for the Detection and Classification of Volatile Organic Compounds. *ACS Applied Materials & Interfaces* **2013,** *5* (8), 3431-3440.

63. Zellers, E. T.; Han, M. Effects of Temperature and Humidity on the Performance of Polymer-Coated Surface Acoustic Wave Vapor Sensor Arrays. *Analytical Chemistry* **1996,** *68* (14), 2409-2418.

64. Falk, M.; Poole, A. G.; Goymour, C. G. Infrared study of the state of water in the hydration shell of DNA. *Canadian Journal of Chemistry* **1970,** *48* (10), 1536-1542.

65. Tao, N. J.; Lindsay, S. M. Structure of DNA Hydration Shells Studied by Raman-Spectroscopy. *Biopolymers* **1989,** *28* (5), 1019-1030.

Chapter 2

MATERIALS AND METHODS

2.1 Electrode Preparation

Two types of substrates were fabricated. 20 μm spacing, circular electrodes (Figure 2.1) were designed to be similar to typical chemiresistor electrodes in literature [1]. 4-inch silicon wafer with 300 nm of thermally grown oxide was used as the substrate. Patterns were defined using standard photolithography, followed by electron-beam evaporation of metal films and lift-off processes. The electrodes deposited were made of 10 nm thick of titanium and 200 nm thick of gold. The circular electrode has a diameter of 2.7 mm with electrode width of 20 μm and pitch width of also 20 μm. Each device chip was 0.4 cm^2 in size and had a single chemiresistor with an area of 23 mm^2. The total electrode perimeter is estimated as 290 mm.

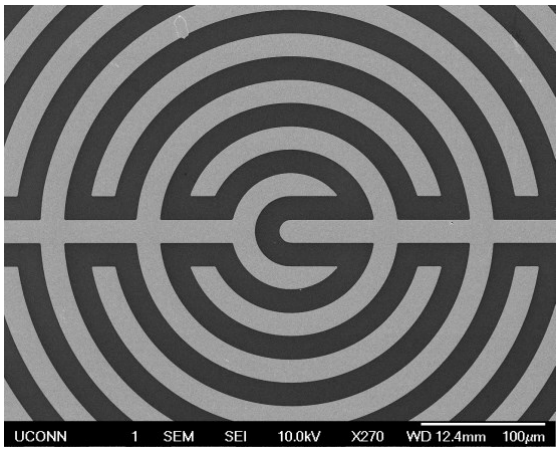

Figure 2.1 Interdigitated circular electrodes with a spacing of 20 µm.

2.2 Sensor Device Preparation

Sensor devices were prepared using solution phase deposition of gold nanoparticles on electrodes. Citrate-stabilized gold nanoparticles (10 nm diameter, OD1), tris-(2-carboxyethyl) phosphine hydrochloride (TCEP), glacial acetic acid, sodium acetate, sodium chloride (NaCl), 1-octanethiol, and 8-mercapto-1-octanol were purchased from Sigma-Aldrich (St. Louis, MO). Tris base was purchased from Fisher Scientific (Suwanee, GA). All aqueous solutions were made with double-distilled water (dd-H_2O). Single-stranded oligonucleotide sequences were purchased from Integrated DNA Technologies Inc (Coralville, IA), and the sequences are shown in Table 2.1.

Table 2.1 DNA Oligomers

name	Sequence (5' to 3')
SEQ 01	/Cy-5[a]/AAA AAA AAA GAG GAG GAA AAG GAG T
SEQ 02	/ThioMC6-D[b]/TTT TTA CTC CTT TTC CTC CTC TTT T
Poly A	/ThioMC6-D[b]/AAA AAA AAA AAA AAA AAA AAA AAA A
Poly T	/ThioMC6-D[b]/TTT TTT TTT TTT TTT TTT TTT TTT T
Poly C	/ThioMC6-D[b]/CCC CCC CCC CCC CCC CCC CCC CCC C
Poly A 10 mer	/ThioMC6-D[b]/AAA AAA AAA
Poly A 50 mer	/ThioMC6-D[b]/A_{50}
24 LOOP	/ThioMC6-D[b]/AAA AGG GGA AAA AAA ACC CCT TTT
24 LINEAR	/ThioMC6-D[b]/GAA TTA ACA AAC CAG ATA ACG ATG

[a] Cyanine fluorescence group

[b] Thiol functionalization group -C_6H_{12}-SH

2.2.1 Preparation of DNA Functionalized Gold Nanoparticles

A number of methods for attaching organic species to gold nanoparticles have been found, including the use of citrate, phosphine, amine, and carboxylate and thiol groups [2]. Of all these methods, thiol-gold chemistry has long been established as the standard method for most gold nanoparticle applications primarily due to the stability of the products. For vapor sensors in particular, the majority of organic layer attachment has been based on thiol-gold chemistry [3]. When the ligand in question is DNA, thiol-based attachment is even more attractive. Compared with random adsorption by the nucleobases, this end-on covalent attachment method is more

stable. Practically, thiol-linked DNA would not fall off during the centrifugation process. This technique is also neat and allows for hybridization with complementary DNA segments [4] and aptamer-based solution-phase specific ligand-receptor interaction [5-6]. Therefore, this behavior is very useful in fluorescence-based characterization of DNA surface coverage [7]. Nevertheless, although DNA-functionalized gold nanoparticles through thiol attachment can be very effective tools for molecular recognition in solution, it remains to be answered whether the conformation of DNA is retained when the nanoparticles are dried. Furthermore, DNA nucleobases are known to nonspecifically adsorb onto gold surface through weak van der Waals nucleobase-gold interactions [8]. This non-specific interaction would possibly alter the DNA conformation from its native state, thereby complicating dry-state DNA-vapor interactions. Thus, the aim of this entire study is realistically not to emphasize vapor phase molecular recognition, but to more of exploring the vapor sensing capability using the chemiresistive transduction mechanism and sequence-dependent vapor distinguishability. It needs to be emphasized that any resulting response differences could be due to conformational differences, chemical differences, or a combination of both. Therefore, it is not the scope of this study to quantify the contribution of chemical and conformational properties towards sensor responses.

SEQ 02, poly A, poly T, and poly C were used to functionalize citrate-stabilized gold nanoparticles following a standard thiol-gold protocol with minor modifications [9]. To activate the thiol-modified DNA sequences, 3 µl of DNA solution (1 mM), 1 µl of acetate buffer (500 mM, pH 5.2) and 1.5 µl of TCEP (10 mM) were mixed with H_2O to obtain a final volume of 10 µl and incubated for 1 hour at room temperature. The mixture was added to 1 ml of as-received citrate-stabilized gold nanoparticle solution and reacted for 16 hours in the dark at room temperature. Subsequently, 10 µl of Tris acetate (500 mM, pH 8.2) buffer was added into the

gold nanoparticle solution, followed by the addition of 110 µl NaCl (1.0 M) dropwise with gentle shaking. The whole mixture was incubated in the dark for another 24 hours before use. In control experiments, H_2O was added to 1 ml of gold nanoparticle solution in place of DNA, prior to the 16-hour incubation step.

2.2.2 Deposition of DNA Functionalized Nanoparticles on 20 µm Circular Electrodes

Excess buffer salts (e.g., NaCl) from DNA-functionalized gold nanoparticle storage solutions were first removed through centrifugation processes. 1 ml of nanoparticle solution was subjected to centrifugation at relative centrifugation force (RCF) = 15,000 *g* for 40 minutes, the supernatant was removed, and the concentrate was re-dispersed in 1.5 ml dd-H_2O. This washing procedure was repeated twice. The final product obtained from centrifugation was suspended in 20 µl of dd-H_2O to form a DNA-functionalized gold nanoparticle concentrate. The concentrate for drop-casting was standardized using a UV-Vis spectrophotometer (Thermo Scientific NanoDrop ND-1000) to have absorbance = 2.5. For drop casting, 4 µl of gold nanoparticle concentrate was deposited on each sensor area. The droplet readily wets the electrode areas, and was evaporated under a dry air atmosphere at room temperature. DC resistances measured in air have a resistivity in the range of 300 to 800 kΩ.

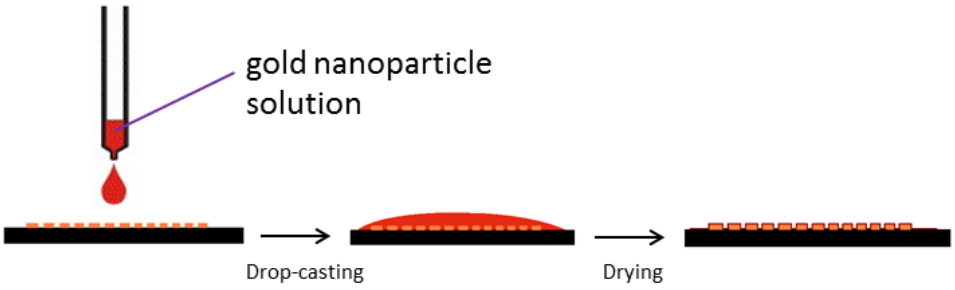

Figure 2.2 Depositing gold nanoparticles by drop casting

2.3 Characterization of Nanoparticles

2.3.1 Fluorescence Quantification of DNA Coverage on Gold Nanoparticles

In solution, SEQ 02 modified gold nanoparticles were studied with the aid of a fluorescence-based method [7]. After preparation of SEQ 02 modified gold nanoparticles, 100 µl of gold nanoparticle solution was washed with dd-H_2O twice by centrifugation at 15,000 *g* for 40 minutes to remove free SEQ 02 DNA. The pellet of gold nanoparticles was subsequently dispersed into 100 µl NaCl solution (100 mM). The concentration of gold nanoparticle solution was determined by measuring the absorbance at 520 nm using a UV-Vis spectrophotometer (Thermo Scientific NanoDrop ND-1000). Afterwards, 1.5 µl of Cy5-labeled SEQ 01 (100 µM) was added to the gold nanoparticle solution to hybridize with the SEQ 02 immobilized on the gold nanoparticles. The mixture was kept in the dark with gentle shaking at room temperature for 2 hours. Two additional rounds of washing with 100mM NaCl solution were carried out, and the unhybridized SEQ 01 in the supernatant was measured after each washing step. The concentration of free SEQ 01 was determined using a fluorospectrometer (Thermo Scientific NanoDrop 3300). The quantity of SEQ 02 chemisorbed on gold nanoparticles approximately equals the amount of SEQ 01 consumed through complimentary base paring. The amount of SEQ 01 consumed due to hybridization was determined as the difference between the initial amount of SEQ 01 added and free, unhybridized SEQ 01 measured in the supernatant, summed from each of the three washings.

$$\text{DNA per AuNP} = \frac{\text{Moles}_{\text{Initial amount of SEQ 01}} - \text{Moles}_{\text{unhybridized SEQ 01}}}{\text{Moles}_{\text{AuNP}}} \qquad (2.1)$$

2.3.2 Characterization of Dry Gold Nanoparticles

DNA-functionalized gold nanoparticles were characterized both in solution and in dried drop-cast forms. Functionalized nanoparticles were first examined with transmission electron microscopy (TEM, FEI Tecnai T12) to verify the nanoparticle size and morphology. To prepare the TEM samples, 1 μl of as prepared DNA-functionalized gold nanoparticles were dropped on a 300 mesh copper grid. After drying, the TEM sample was imaged under an accelerating voltage of 120 kV. Surface characterization of dried DNA-functionalized gold nanoparticle films was also performed using X-ray photoelectron spectroscopy (XPS) (Kratos AXIS 165) with a monochromatic Al-Kα X-ray source. The importance of surface characterization is to verify that using the thiol-gold chemistry, the quantity of DNA adsorbed onto gold nanoparticles is not greatly influenced by the DNA sequence differences. Gold nanoparticle concentrates after centrifugation and washing were drop-cast on oxygen-plasma treated indium foils before insertion in to the XPS vacuum chamber. Surface analysis was performed on both DNA-functionalized gold nanoparticles and control nanoparticles without DNA to measure elemental composition. The DNA coverage obtained from SEQ 02 characterization was used as a reference for estimating poly A, poly T, and poly C coverage with XPS. This was done by comparison of the N and P elemental percentages with SEQ 02 as a reference. The peak area of each element's major peaks in the XPS spectra was used with documented sensitivity factors to calculate the compositions of the sample surface using the following relationship [10]:

$$C_A = \frac{A_A/S_A}{\sum_n A_A/S_A} \tag{2.2}$$

After sensor device fabrication, film morphology was characterized using scanning electron microscopy (JEOL JSM-6335F FE-SEM). Local chemical composition analysis was performed using energy dispersive x-ray spectrometry (EDX) at an excitation voltage of 15 kV. Electrochemical impedance spectroscopy (EIS) measurements were performed using an electrochemical workstation (CH Instruments 660D) under a two-electrode setting with a testing range of 0.1 Hz to 100 kHz.

2.3.3 IV Curve Measurements

IV curves of sensor devices were taken using a source measurement unit (Keithley 2612) controlled by a LabView program. All IV curves taken were triangular sweeps, including a ramp up from 0 V to high voltage, down to a negative high voltage, and back to 0 V. Ramp rate was kept at 0.1 V/s. IV curves were taken for poly A DNA-functionalized gold nanoparticles on 20 μm devices.

2.4 Vapor Sensing Tests

A custom-built dedicated vapor delivery and testing system was used for vapor testing, as shown in Figure 2.3. The vapor delivery system is capable of delivering a mixture of two vapors mixed with carrier nitrogen gas. One of the vapors is the organic vapor of interest; the other vapor is water vapor, used for humidity control. With the use of a flowrate adjustment line, the total flowrate during testing can be kept constant while vapor lines are switched on and off. Therefore test mixtures with constant flowrates and fixed partial pressures of the vapor being tested can be generated.

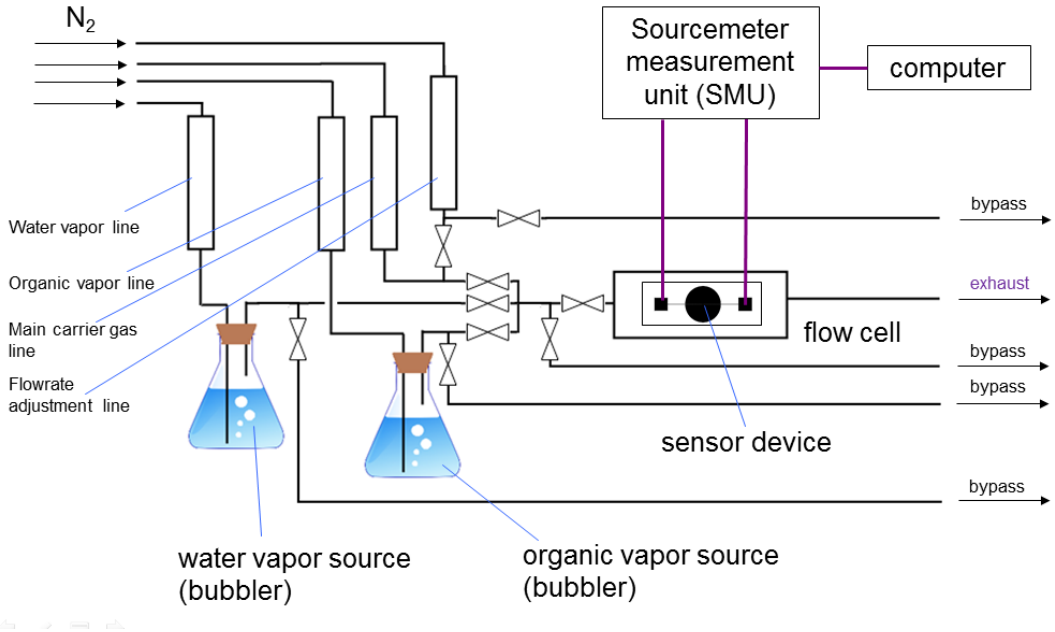

Figure 2.3 Schematics of vapor delivery and testing system

For sensing experiments, sensor devices were wire-bonded (West Bond 747630E) to a two-pin chip carrier. The two terminals of each chip carrier were connected to a source measurement unit (Keithley 2612). The chip carrier was fitted onto a custom built 0.5 cm × 2 cm x 15 cm flow cell fabricated from aluminum and sealed with o-rings. The flow cell allows concurrent testing of up to 8 devices, with an effective chamber volume for each sensor of approximately 2 cm^3. The source measurement unit was programmed to generate a 1.0 V_{pp} square wave at 500 Hz, and DC current was recorded in the middle of each positive half-cycle. Data collection was performed using a LabView program controlling source measurement unit. Ultrahigh purity nitrogen (Air Gas, purity of 99.99%) was used as a diluent and carrier gas. Saturated water and organic vapors were generated using bubblers.

2.4.1 Testing Organic Vapors in a Dry Condition

For studies on sensor response to dry organic vapor analytes, only the main carrier gas line, vapor line, and flowrate adjustment lines were used. Total flowrates were kept at 620 cm^3/min.

2.4.2 Testing Organic Vapors in the Presence of Water Vapor

For studies of the effect of humidity on sensor response, all four input lines were used. Seven relative humidity (RH) levels were investigated: 0 %, 17 %, 34 %, 50 %, 67 %, 84 % and 100%, with a total flow rate of 600 cm^3/min. The effect of RH on sensor response to organic vapors was measured at 0 %, 17 %, 34 %, 50 %, 67 %, 84 %, and 99%. Due to the inclusion of additional gas streams, the total flow rate was 620 cm^3/min. Organic vapor levels are quantified as the ratio of the vapor partial pressure to its saturation vapor pressure (p/p_0) at 22 °C. For measuring the device response to organic vapors, special care was taken to maintain a constant water mole fraction in the gas phase. This was necessary to avoid sensor responses from changes in the humidity of the input flow streams. In all vapor sensing experiments, a steady baseline was achieved before adding organic vapors. After each experiment, the sensors were purged by humidified nitrogen of the specified RH for 5 minutes followed by dry nitrogen for 5 minutes. The sensors were then stored in dark containers filled with N_2 to minimize light-induced and oxidative damage. All experiments were carried out at an ambient temperature of 22 ± 1 °C.

2.5 References

1. Peng, G.; Tisch, U.; Adams, O.; Hakim, M.; Shehada, N.; Broza, Y. Y.; Billan, S.; Abdah-Bortnyak, R.; Kuten, A.; Haick, H. Diagnosing lung cancer in exhaled breath using gold nanoparticles. *Nat Nano* **2009,** *4* (10), 669-673.

2. Daniel, M.-C.; Astruc, D. Gold Nanoparticles: Assembly, Supramolecular Chemistry, Quantum-Size-Related Properties, and Applications toward Biology, Catalysis, and Nanotechnology. *Chemical Reviews* **2003,** *104* (1), 293-346.

3. Ibañez, F. J.; Zamborini, F. P. Chemiresistive Sensing with Chemically Modified Metal and Alloy Nanoparticles. *Small* **2012,** *8* (2), 174-202.

4. Mirkin, C. A.; Letsinger, R. L.; Mucic, R. C.; Storhoff, J. J. A DNA-based method for rationally assembling nanoparticles into macroscopic materials. *Nature* **1996,** *382* (6592), 607-609.

5. Huang, C.-C.; Chiu, S.-H.; Huang, Y.-F.; Chang, H.-T. Aptamer-Functionalized Gold Nanoparticles for Turn-On Light Switch Detection of Platelet-Derived Growth Factor. *Analytical Chemistry* **2007,** *79* (13), 4798-4804.

6. Tan, D.; He, Y.; Xing, X.; Zhao, Y.; Tang, H.; Pang, D. Aptamer functionalized gold nanoparticles based fluorescent probe for the detection of mercury (II) ion in aqueous solution. *Talanta* **2013,** *113* (0), 26-30.

7. Demers, L. M.; Mirkin, C. A.; Mucic, R. C.; Reynolds, R. A.; Letsinger, R. L.; Elghanian, R.; Viswanadham, G. A Fluorescence-Based Method for Determining the Surface Coverage and Hybridization Efficiency of Thiol-Capped Oligonucleotides Bound to Gold Thin Films and Nanoparticles. *Analytical Chemistry* **2000,** *72* (22), 5535-5541.

8. Opdahl, A.; Petrovykh, D. Y.; Kimura-Suda, H.; Tarlov, M. J.; Whitman, L. J. Independent control of grafting density and conformation of single-stranded DNA brushes. *Proceedings of the National Academy of Sciences* **2007,** *104* (1), 9-14.

9. Liu, J.; Lu, Y. Preparation of aptamer-linked gold nanoparticle purple aggregates for colorimetric sensing of analytes. *Nat. Protocols* **2006,** *1* (1), 246-252.

10. Moulder, J. F.; Chastain, J. *Handbook of X Ray Photoelectron Spectroscopy: A Reference Book of Standard Spectra for Identification and Interpretation of XPS Data*; Physical Electronics Division, Perkin-Elmer Corporation 1995.

Chapter 3

RESULTS AND DISCUSSION

3.1 Characterization of Gold nanoparticles and Sensor Devices

As with all other sensors, the properties of the active sensing materials determine the sensor's sensing mechanism and performance. Organothiol-functionalized nanoparticles have been commonplace in gold nanoparticle chemiresistive sensing materials [1], and their properties in dry form were well-characterized even before they were used as a sensing material [2]. However, for the relatively new DNA-functionalized nanoparticles, reported applications have essentially been in aqueous solutions [3]. To demonstrate they are a useful material in the dry phase, surface characterizations in addition to solution phase ligand coverage analysis is needed to understand its ligand quantity and stability as a dry material. Therefore for DNA-functionalized gold nanoparticles, fluorescence analysis and XPS analysis were used in a complementary way to examine surface coverage for all DNA sequence on gold nanoparticles.

3.1.1 Characterization of Gold nanoparticles

Although the main objective is to use gold nanoparticles for sensing, it is important to first qualify the nanoparticles as suitable starting material for integrating with sensor devices. The aim of all characterization work done was to ensure that the nanoparticles have been successfully functionalized before deposition and they have the right morphology. A complementary solution and dry phase characterizations were needed to provide evidence that

surface functionalization was successful and equal across all different sequences. While solution-phase fluorescence characterization provides a more accurate estimate of the surface ligand coverage, surface XPS characterization of the dry material allows a comparison of surface chemical composition across all different samples. As will be seen in Section 3.2, sensing comparison would only be meaningful when the surface coverage of DNA on nanoparticle surfaces was identical.

3.1.1.1 TEM Analysis of DNA-Functionalized Gold nanoparticles

TEM image of the DNA-functionalized gold nanoparticles showed average diameter of 10 nm. Both samples of gold nanoparticles show no sign of particle coagulation on a dried carbon film. The morphology of these discrete nanoparticles were close to small molecule organothiol-functionalized gold nanoparticles used in previous studies [4]. Therefore it is expected that they perform similarly as their organothiol functionalized gold nanoparticles counterparts.

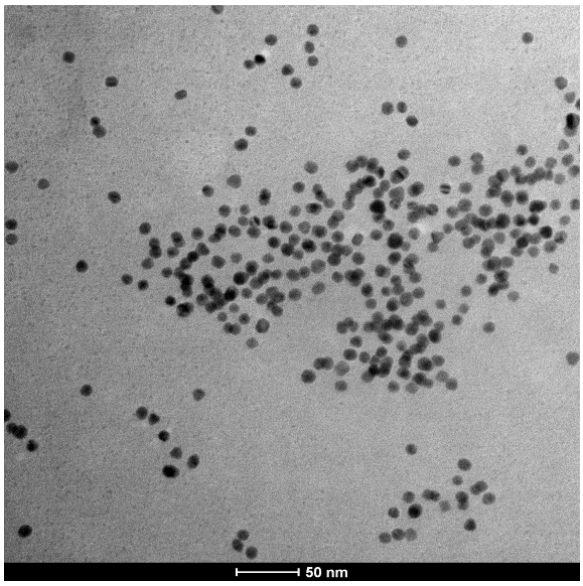

Figure 3.1 TEM images of 10 nm DNA-functionalized gold nanoparticles

3.1.1.2 DNA-Functionalized Gold nanoparticles

The attachment of thiol-functionalized DNA to gold nanoparticles was apparent from visual inspection. For all sequences studied, DNA-functionalized gold nanoparticles were observed to maintain good dispersion in solution. By contrast, addition of buffer solution to citrate-stabilized gold nanoparticles without DNA resulted in nanoparticle aggregation within a few hours. A change in solution color from light red to light purple was an indication of aggregation. These observations are consistent with superior stabilization of DNA-functionalized nanoparticles in electrolyte solutions through synergistic electrostatic and steric mechanisms [5]. Gold nanoparticles with citrate capping alone are known to be less resistant to aggregation as they are predominantly electrostatically stabilized [6]. For SEQ 02, the fluorescence-based technique shows that surface coverage is 40 (± 6) DNA oligonucleotides per nanoparticle. For 10 nm diameter particles, the surface density is 1.3 x 10^{13}/cm^2, which can be

compared with literature data: 5 x 10^{12}/cm^2 [7] and 3.7 x 10^{13}/cm^2 [8-9] for 25-mers, and 1.4 x 10^{13}/cm^2 for a 15 mer [10]. Previous studies have shown that ss-DNA oligomers of 25 mer size are generally coiled structures that extend 0.7 to 1.0 nm from the particle surface [11-13].

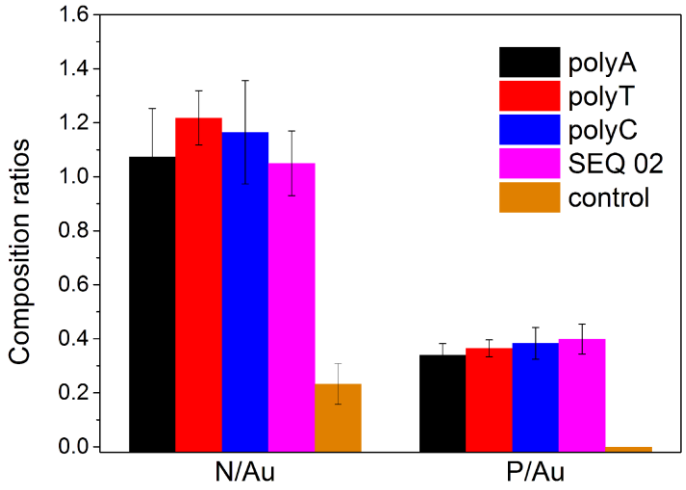

Figure 3.2 Surface composition of nitrogen and phosphorus on DNA-functionalized gold nanoparticles compared to controls with citrate-capped gold nanoparticles; control samples have no P signal.

Surface analysis was performed with XPS to verify that DNA is present on all gold nanoparticle films after drop-casting and drying. Figure 3.2 shows measurements of nitrogen and phosphorous content for DNA-functionalized gold nanoparticles compared with control samples. Nitrogen contents of all DNA-functionalized samples were within the range of 3 ~ 4 % and phosphorous was approximately 1 %. Due to the minute amount of sulfur per molecule, no Sulfur 2p signals were observed on any sample [8]. The phosphorous signal from the DNA-functionalized gold nanoparticle films serves as direct evidence of successful DNA adsorption

onto nanoparticles. No phosphorous is measured on control samples. There is a small N 1s signal from control samples that may originate from residual buffer salts, but the DNA samples have a 3× higher N 1s signal that is consistent with DNA coverage of the gold nanoparticles. Estimates of surface coverage for poly A, poly T, and poly C- functionalized gold nanoparticles are obtained by comparing XPS surface phosphorous percentages to SEQ 02 as a reference. Results are 42, 36, and 36 molecules per particle for poly A, poly T, and poly C, respectively. Other elemental signatures such as C and O were not useful for distinguishing DNA and control samples.

3.1.2 Sensor Device Characterization

SEM was used as the primary tool to look at deposited gold nanoparticle films on electrode surfaces. The most useful information it conveys is the uniformness, continuity and location of deposited films. As drop-casting was not intended as a monolayer deposition technique, the nanoparticle films were probably multilayers, and SEM was not an ideal tool to tell whether the nanoparticles had coagulated during drying and device aging. It will be left to a later section of electrical measurements to provide more direct information of the quality of nanocomposite films formed.

Due to macroscopic fluid mechanics effect and coffee ring effect [14], the films of nanoparticles deposited on sensor substrates are usually not of uniform thickness, as shown in Figure 3.3(a). DNA-functionalized gold nanoparticles deposited on circular electrodes with 20 μm gaps were examined with SEM and are displayed in Figure 3.3(b). Independent of the DNA sequences being used, the nanoparticles were able to form a nearly continuous film structure

across the gold fingers on the substrates, covering most of the circular electrode area. On certain parts of the electrode (<10% of total area) where nanoparticle coverage was very low, the electrode could be performing as an open circuit, thus not contributing to the total current. However, these "dead" areas were not observed to adversely affect the sensor performance.

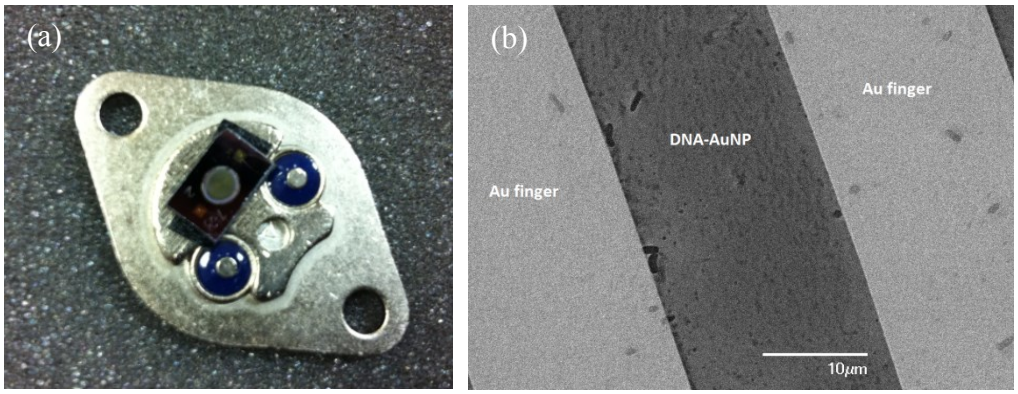

Figure 3.3 (a) Colored photo of a 20 μm gap sensor device with DNA-functionalized gold nanoparticle coverage and mounted on a chip carrier; (b) SEM images 20 μm gaps filled with DNA-functionalized gold nanoparticles

3.1.3 I-V Curves

I-V curves, or current-voltage characteristics, are usually the preliminary and one of the most important characteristics of any electrical devices. They provide information on electrical conduction mechanisms and film structure. Figure 3.4 shows the I-V curve of a 20 μm device with poly A DNA-functionalized gold nanoparticles collected with a pure N_2 flow at 600 cm^3/min. On the 20 μm DNA-functionalized gold nanoparticle sensor devices, the I-V curves are both approximately linear and are ohmic type, regardless the materials deposited on it.

Joseph et. al. conducted a study on the effect of layer number on the I-V curves with 1,12-dodecanedithiol-functionalized gold nanoparticles [15]. He reasons that the nanoparticle film has a percolation threshold for electrical conduction. When the film is very thin, the individual clusters of nanoparticles are far away from each other and the film is not conductive. When the film is close to the percolation threshold, large islands of nanoparticles are present. Within a large island, as the inter-particle distances are very small and the capacitances are also small, the entire island behaves like a resistor. However, islands are separated by nanosized gaps of higher capacitance which are bottleneck junctions in the 1-dimensional percolation pathway. These bottlenecks are single-electron-charging barriers in the percolation pathways. As these gaps dominate the charge transport, a tunneling-like I-V behavior is observed. The origin of the non-linearity in the observed I-V curves can be explained by a multitude of bottleneck junctions whose capacitances are different within the film. This assembly of tunnel junctions of varying energy barriers averaged out the Coulomb blockade behavior of individual junctions, thus giving rise to a smoothened S-shaped I-V curve. When the nanoparticle layers become thicker, the percolation threshold is overcome. A complete nanoparticle network with small inter-particle distances is formed, hence no bottleneck junction effect is absent. The film behavior becomes purely resistive, resulting in a linear I-V curve.

For DNA-functionalized gold nanoparticle sensors, the film nanoparticle films formed are of various thicknesses across the device surface, with certain areas covered by multiple layers of nanoparticles. Therefore a well-interconnected nanoparticle network is dominates the electrical conduction and the I-V curve is typically linear.

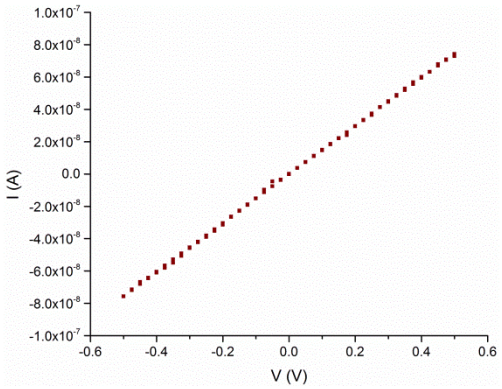

Figure 3.4 I-V curves of a 20 µm device with poly A DNA-functionalized gold nanoparticles

3.2 Vapor Sensing

Vapor sensing experiments were conducted in a customarily designed vapor sensing chamber, a design universally followed by the vapor sensor community. The most important parameters of any vapor sensing experiments are the sensing chamber volume and gas stream flowrates. Together, they define the residence time τ, as

$$\tau = \frac{V}{q} \tag{3.1}$$

where V is the volume of the sensing chamber in cm^3, and q is the volumetric flow rate of the gas stream in cm^3. For a sensing chamber with a flow rate of 600 cm^3/min, and volume for each sensor at 2 cm^3, the τ = 0.2 seconds. This is the time it takes for the atmosphere around the sensor to change from, for example, a clean N_2 stream to one with a certain concentration of toluene vapor. In a perfect sensor test system, a kinetically ideal sensor, which is one that is immediately saturated with the vapor analyte immediately, would reach a saturating response within 0.2 seconds. In the real-time vapor sensing plot, longer time to reach equilibrium could

be the result of three effects. First is the non-ideal vapor adsorption kinetics, one that arises from certain amount of time needed for the sensor to reach equilibrium with the environment. Second is the non-ideality in the vapor stream boundaries. Vapor analytes are diffusive within the flowing gas stream. As there is no sharp boundary between a clean N_2 and a vapor stream, there might be a delay of the onset of the set-point vapor concentration. Third is the non-ideality of the vapor delivery system. As the test chamber does not have the ideal geometry of a perfect small-volume flow path, some vapor dilution may take place initially, and a certain amount of time is needed for the vapor concentration in the chamber to reach equilibrium. Therefore, it is common to observe a gradual increase in sensor response as vapor is introduced into the test chamber by switching of valves. Sensor responses are expressed as the commonly used $\Delta R/R$ where R is the baseline resistance of the sensor at a given RH, and ΔR is the vapor induced change from the baseline.

In this study, R/R_0 is used to characterize the ratio of resistance at a specific RH to the resistance at RH = 0%, and $\Delta R/R$ is used to characterize sensor response to analytes at fixed RH. Water vapor is not treated as an analyte, but as an environmental factor that modifies the baseline resistance of the sensor at a specific RH. R_0 is the sensor baseline resistance at zero RH or in a dry atmosphere.

3.2.1 Vapor Sensing under Dry Conditions

Responses of sensors with different DNA sequences were measured concurrently under each organic vapor to improve sequence-to-sequence comparability. Figure 3.5 shows the response of 4 different DNA gold nanoparticle sensors to hexane at three vapor concentrations. The plots show a rapid response, good reversibility, and near-linear dependence on hexane vapor

pressure. All four sequences show a response to hexane vapor, but there are clear sequence-dependent intensity differences. SEQ 02 and poly C have the largest response, while poly T has the smallest. Positive ΔR/R values are indicative of a swelling-dominated behavior.

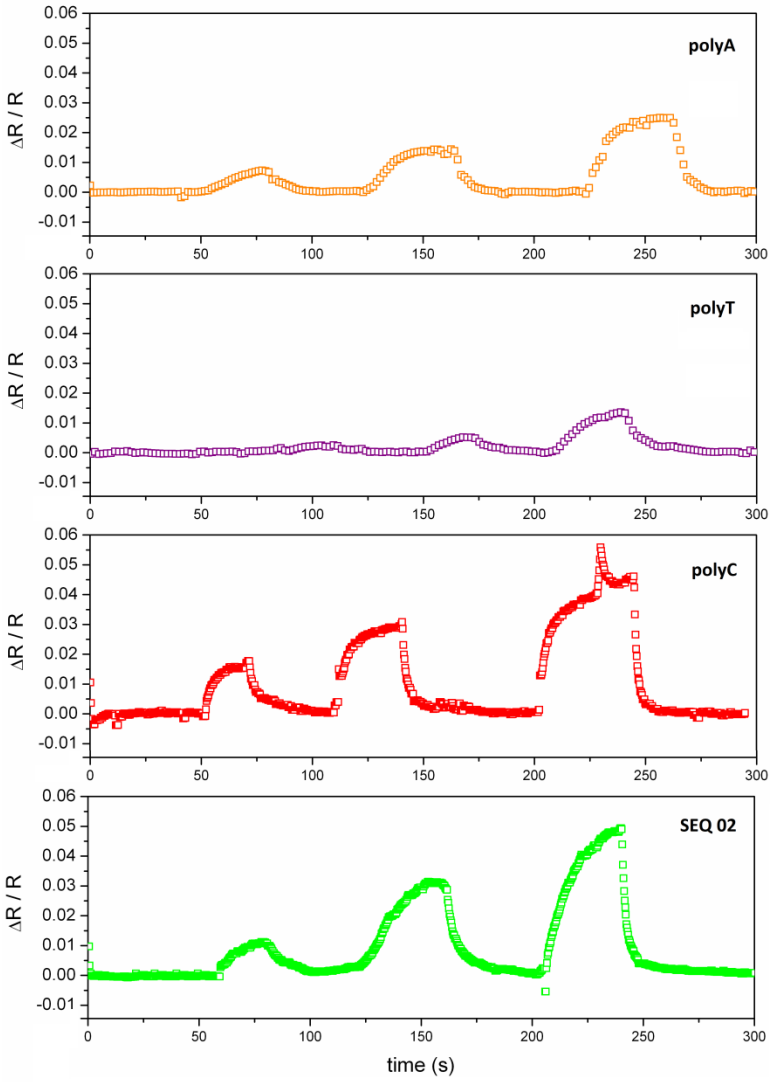

Figure 3.5 Real-time response of 4 types of DNA-functionalized gold nanoparticle sensors on hexane vapor at RH = 0% with $p/p_0 = 0.012$, 0.024 and 0.036.

Figure 3.6 is a combined plot of sensors to all five organic vapors. ΔR/R values are all positive, which is consistent with alkanethiol-functionalized gold nanoparticle chemiresistive sensors [16], indicating a swelling-dominated behavior. Considering that the DNA oligomers on the gold nanoparticle surfaces have identical length, this sequence-dependent response difference is remarkable. Although chemometric analysis is not a goal of this study, it can be commented that pattern recognition methods could probably be used with a DNA-functionalized gold nanoparticle sensor array to effect vapor identification capabilities.

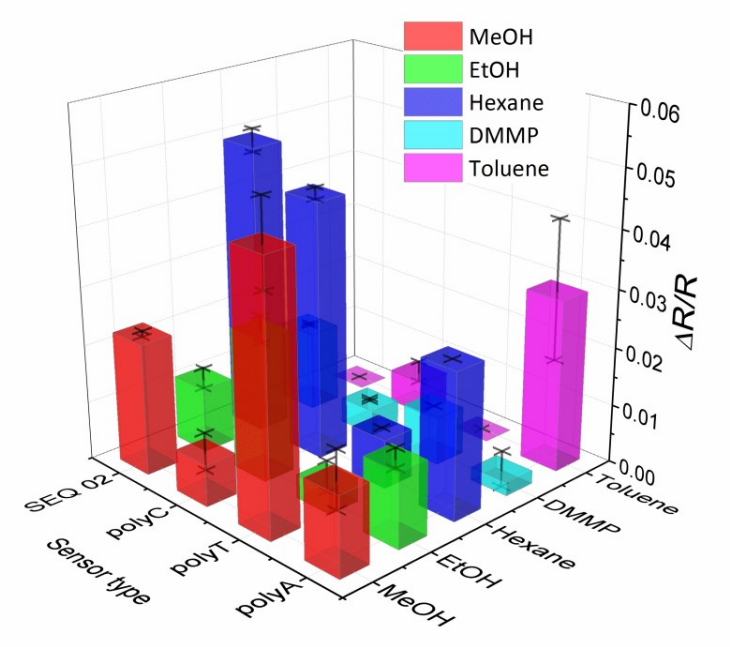

Figure 3.6 3D bar chart of responses of 4 sensors to 5 vapors at $p/p_0 = 0.036$

3.2.2 Relative Humidity Effects

To study the effects of relative humidity, it becomes imperative to understand the effect of water vapor alone on sensors. As stated early in Chapter 1, humidity effects would affect hydrophilic DNA molecules to a great extent. Therefore the study of sensitivity to water vapor

forms a standalone study, and the results of the sensitivity to water vapor are correlated to sensor's behavior towards organic vapors in the next study.

3.2.2.1 Sensitivity to Water Vapor

For all sensors, R/R_0 increases from 1 at RH = 0% to around 2 at 34%, and then decreases rapidly, reaching 0.01 above RH = 50% (Figure 3.7a). This dichotomous behavior is atypical for nanoparticle-based chemiresistive sensors. This can be seen by comparing water vapor sensing behavior between DNA-functionalized gold nanoparticles and alkanethiol-functionalized gold nanoparticles. To that end, 1-octanethiol and 8-mercapto-1-octanol functionalized gold nanoparticle sensors were prepared using the standard protocol by Woltjen et al. [16] and subjected to identical vapor testing conditions. The R/R_0 trends with increasing RH for these devices are shown in Figure 3.7b. The monotonic trends are similar to previously published gold nanoparticle chemiresistive sensors with alkanethiol-type ligands [16-17]. Similarly, studies of pure DNA films also report monotonous resistivity trends across the RH range from 0% to 100% [18]. The distinctive behavior of DNA-gold nanoparticle films is therefore an indication that the conduction mechanism of DNA-gold nanoparticle films has contributions from both nanoparticles and the polyelectrolyte matrix.

The distinctive response of DNA gold nanoparticle devices can be understood from two separate conduction mechanisms. At low RH levels (0% to 40%), the upward trend in R/R_0 is governed predominantly by matrix-swelling effects common to gold nanoparticle chemiresistive sensors. In this RH range, the effects of ionic conduction are insignificant compared to the electronic current. At higher RH levels (40% to 100%), ionic conduction becomes significant and R/R_0 decreases. Similar effects of decreasing resistivity at higher vapor concentrations have been observed in studies of tetraoctylammonium bromide (TOAB) functionalized gold

nanoparticles [19-20]. In that study, residual ionic species solvated by vapors were proposed as one possible source of increasing conductance. The difference here is that DNA intrinsically contains ionic species that may contribute to conductivity at high RH levels. Voids in the film may also contribute to ionic conduction, as water condensation on the hydrophilic SiO_2 surface under high RH levels is likely [21].

The significant response to increasing humidity for all ss-DNA devices studied is indicative of the favorable hydration of DNA oligomers. Water is integral to DNA structure with significant interactions at both phosphate and base sites, and the hydration shell has been described as a monolayer of water on the DNA surface area [22]. Estimates for hydrated ds-DNA are near 30 H_2O per nucleotide pair with waters strongly bound even at 0% RH [23]. Base specific interactions have been observed in crystallographic studies but these effects are complicated by structure [24]. For example, it was reported that the strength of water interaction first decreases, but then increases with increasing AT content [22]. In Figure 3.7a, SEQ 02 has the strongest response to water even though it has significant T content and poly T has the weakest response. Further study is needed to separate base composition from sequence and structure effects.

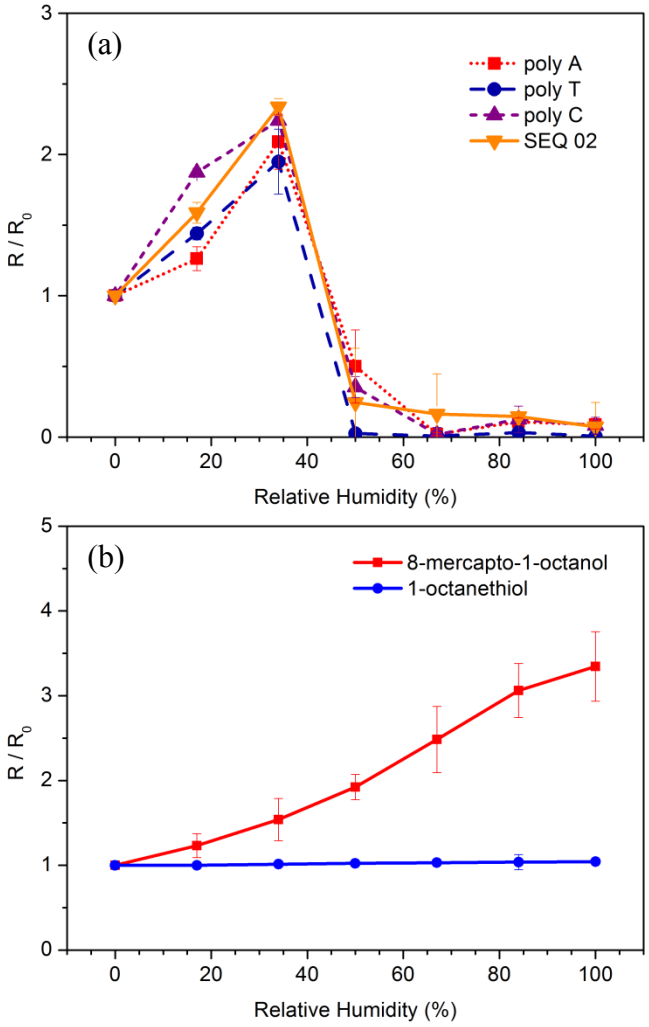

Figure 3.7 (a) Effect of RH on baseline resistance of DNA-functionalized gold nanoparticle films; (b) Effect of RH on resistance of two types of alkanethiol-functionalized gold nanoparticle films.

IV curves of DNA functionalized gold nanoparticle sensors provided additional evidence for the mechanism change. At low relative humidities from RH = 0% to 33.3%, a linear I-V curve was obtained, while for RH = 45.5% to 57.1% a hysteresis loop was obtained. The switch from a linear I-V plot to a curved hysteresis loop was attributed to the appearance of any

capacitance in the material. Capacitance of a similar kind was reported for carbon-based ionic conduction humidity sensors, and this effect has been attributed to the activation of mobile ions in the film and consequently double layer effects at the electrode/film interface [25]. In gold nanoparticle systems, this behavior was also observed for TOAB functionalized gold nanoparticles [19], on which the bromide ions could act as the mobile charge carriers, leading to ionic conduction.

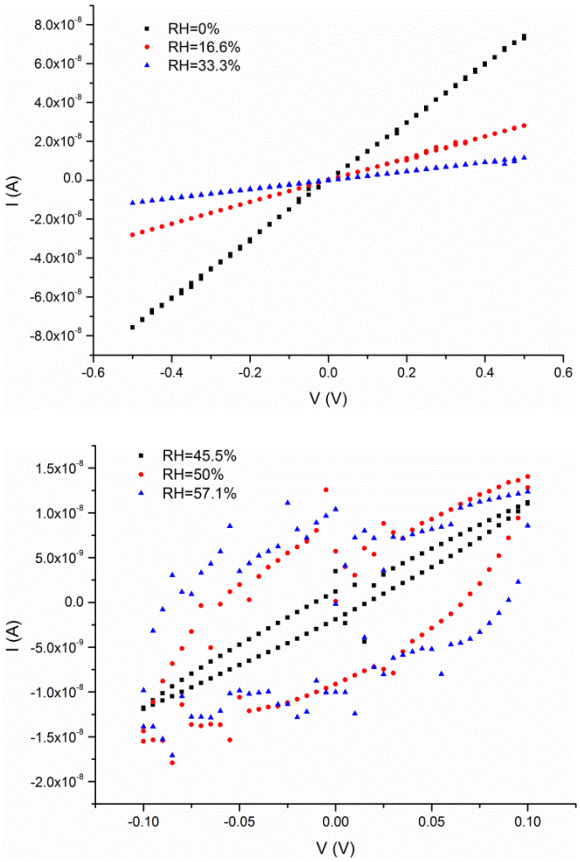

Figure 3.8 I-V curves of a poly A gold nanoparticle functionalized gold nanoparticle sensor under N_2 atmospheres of various relative humidity

To further characterize the conduction mechanisms, electrochemical impedance spectroscopy (EIS) measurements were performed. The EIS results are consistent with a RH dependent conduction mechanism (Figure 3.9). At low RH levels, only a single semicircle is observed on the Nyquist plot, indicating an electron-transfer-limited process [26]. At higher RH levels of 50% for poly A, a linear response appears in the low frequency region, which is characteristic of a diffusion-limited charge transfer process. The source of this diffusion limited charge transfer is a frequency-dependent ion diffusion/ transport in the polyelectrolyte (DNA) [26]. As RH increases, the semicircle radius first increases and then decreases – a trend that corresponds closely with the DC resistance measured using the source measurement unit. In the range of RH from 84% to 100%, the linear portion of the curve becomes increasingly vertical, indicating increasing capacitive behavior, which confirms the dominance of ionic conduction [27]. These Nyquist plots substantially reflect the transition from electronic to ionic conduction as RH increases. DNA-functionalized gold nanoparticle sensors display a distinctive dichotomous behavior in response to RH.

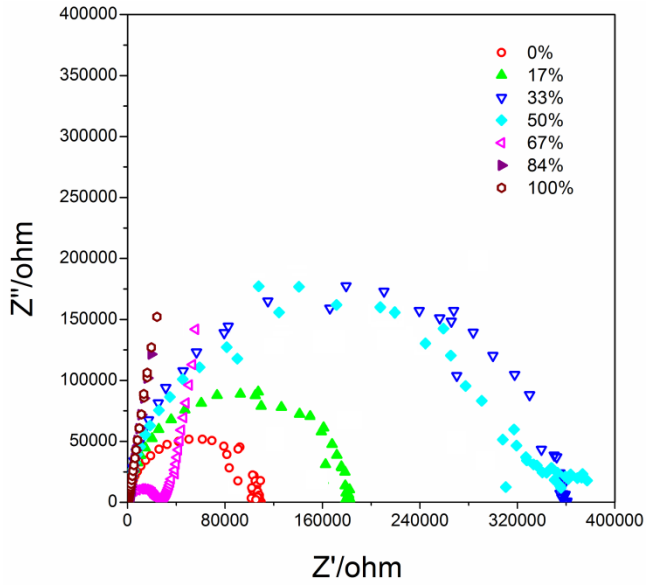

Figure 3.9 Nyquist plots recorded for poly A RH levels 0 to 100%.

3.2.2.2 Sensitivity to Organic Vapors at Various Relative Humidities

Responses to several organic vapors were measured at constant RH for a range of different RH conditions. Figure 3.10 shows the real-time sensor response of SEQ 02 to ethanol at different RH levels. Both positive and negative responses are observed, depending on RH, with a trend towards negative ΔR/R response at increasing RH. The SEQ 02 data show no significant response for the two highest RH values.

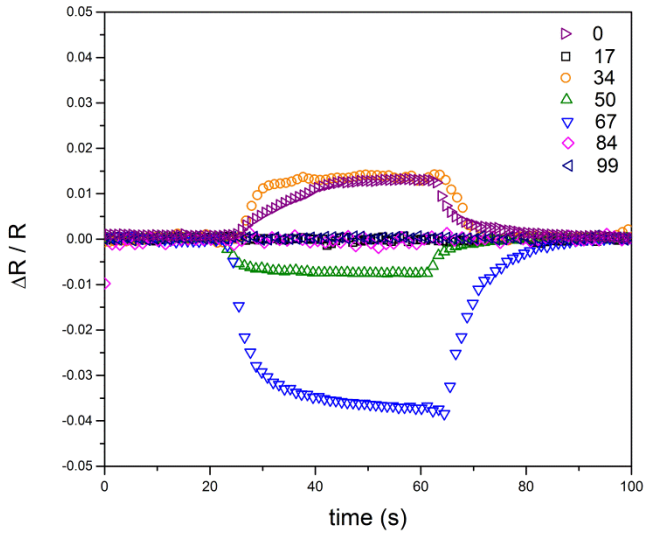

Figure 3.10 Real-time response of a SEQ 02 sensor against ethanol vapor equivalent to $p/p_0 =$ 0.036 at 7 RH levels ranging from 0% to 99%.

Combination plots of sensor responses to all organic vapors at different RH levels are shown in Figure 3.11. ΔR/R values are all positive (downward in the figure) when water vapor is not present, indicating a swelling dominated behavior. These positive responses are similar to that of water vapor Figure 3.7a. However, mostly negative ΔR/R responses are observed for RH in the range of 50% to 67%, while reduced responses are observed in the ranges of RH = 17% to 34% and 84% to 100%. The response patterns are sensitive to RH with highest sensitivity in the range of 50% to 67%. Interestingly, this region is near where the sensitivity to water vapor peaks and then rapidly decreases, although the correlation is not simple. Qualitatively, the response patterns are similar for each of the different DNA sequences with sensitivities that peak in the same regions, but there are sequence dependent patterns that distinguish each different DNA oligomer at a given RH as well as different patterns with RH. For example, poly A has the strongest peak response to all vapors, but the RH dependence is different for each vapor.

Absolute values of response signals vary between different devices, but the qualitative trends are reproducible.

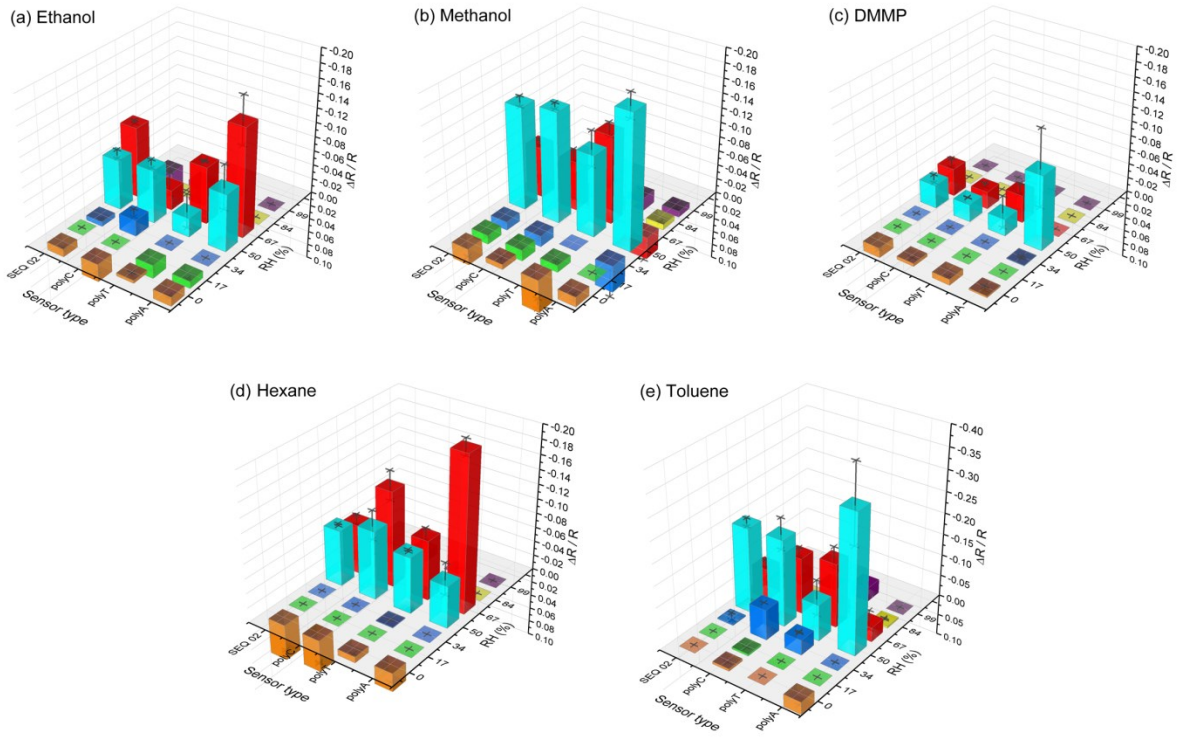

Figure 3.11 3D bar charts of sensor response to 5 vapors across all RH levels (0% ~ 99%) for (a) ethanol; (b) methanol; (c) DMMP; (d) hexane; (e) toluene. Concentrations are $p/p_o = 0.036$ for all five vapors.

In field applications, cross-sensitivity to water is a complicating issue for sensors that function by vapor absorption into a condensed phase. Previous studies with SAW sensors have investigated the effects RH has on baseline and sensitivity towards organic vapors [28]. Similar effects are observed here in DNA functionalized gold nanoparticle chemiresistive sensors, but

the volcano shaped response is distinctive from previous studies with alkanethiol gold nanoparticles that generally report weakening sensor response with increasing RH [20]. This behavior can be rationalized based on hydration and chain flexibility and their influence on the conduction mechanism. In a dry state, the sensor response is primarily from swelling of the composite organic-gold nanoparticle matrix, similar to alkanethiols, and we do not expect significant conformational changes in DNA upon adsorption of organic vapors. The weak response sensitivity for the range of RH levels from 17% to 34% is unexpected since it is weaker than both the dry state and intermediate humidity. It may be that at low RH water is held so tightly by the DNA so as to exclude organic sorption. The water may alter the DNA matrix to be more hydrophilic resulting in weaker interactions with hydrophobic molecules like hexane, as seen in Figure 3.11. At higher RH in the range of 50% to 67%, the DNA becomes hydrated and vapors may displace weakly held water, yielding an enhanced response. At the highest RH levels approaching 100%, sensitivity appears to decrease significantly. The decrease is most likely caused by an increasing ionic conduction contribution that is insensitive to vapor sorption. Representative effects of RH levels on sensor response for a range of analyte concentrations are shown in Figure 3.12. The data reflect similar trends as Figure 3.11. Under dry conditions sensors respond linearly with resistance proportional to concentration, and resemble swelling-dominated alkanethiol-gold nanoparticle chemiresistive sensors [16, 19, 29]. At higher RH values, resistance decreases proportional to concentration, except at 17, 84, and 99% RH where the responses are muted.

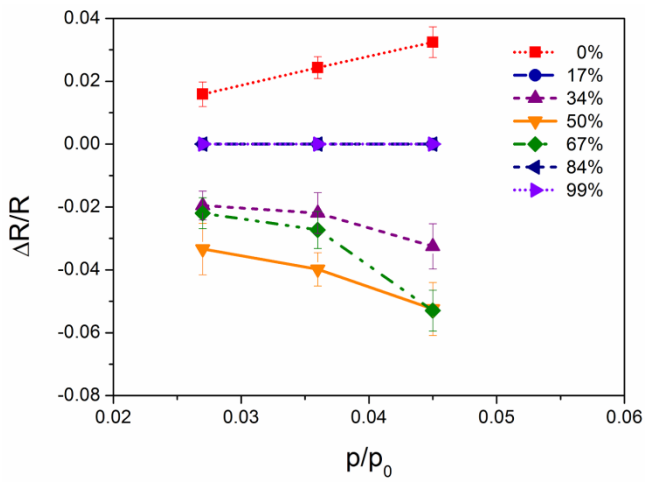

Figure 3.12 Effect of RH levels on responses towards ethanol at p/p_o = 0.027, 0.036 and 0.045 on a set of poly C sensors.

As mentioned earlier, resistance reductions upon vapor sorption have also been reported for TOAB/gold nanoparticle mixtures for both polar and non-polar vapors [19]. It was speculated that solvation effects may increase ion mobility or cause restructuring of the gold nanoparticle film to enhance conductivity. Decreased resistance has also been observed in some alkanethiol functionalized gold nanoparticles for sensing of polar molecules like water and alcohols [16, 29]. Water vapor, in particular, could enhance ionic conductivity from impurities in films [30]. An explanation for the negative ΔR/R regions observed here is possibly more complicated since in addition to previously offered explanations there is the possibility of ligand-binding induced release of water from the hydration shell around the DNA.

3.2.3 Sensitivity and Limits of Detection

Sensors fabricated with this method typically have a root-mean-square (rms) baseline noise on the order of 0.2% ~ 0.3% that is not strongly dependent on humidity. Table 3.1 summarizes the sensitivity for the 4 types of sensors at two working conditions with RH levels of

zero and 50%. Table 3.2 compares limits of detection (LOD) for ss-DNA with organothiol gold nanoparticle sensors that have been widely studied in the literature. For direct comparison, vapor concentrations have been converted to part-per-million. Depending on the analyte, reported LOD values range from a few to a few hundred ppm [1]. Qualitatively, LODs of ss-DNA gold nanoparticle sensors in both dry and humid atmosphere are comparable to organothiol gold nanoparticle sensors. Intermediate RH levels appear to improve the LOD values for the DNA based sensors.

Table 3.1 Sensitivity of 4 types of DNA-gold nanoparticle sensors to 5 vapors at two RH levels

		Sensitivity [a]			
RH (%)	Vapor	poly A	poly T	poly C	SEQ 02
0	Ethanol	0.35	0.11	0.92	0.31
	Methanol	0.14	0.44	0.20	0.75
	Hexane	0.69	0.23	1.22	1.37
	DMMP	0.00	0.23	0.12	0.38
	Toluene	0.82	0.19	0.35	0.23
50	Ethanol	-2.17	-0.72	-1.06	-1.91
	Methanol	-9.45	-3.09	-7.85	-7.64
	Hexane	-1.59	-2.13	-4.50	-3.50
	DMMP	-2.83	-0.64	-0.66	-0.90
	Toluene	-9.03	-2.36	-5.64	-5.58

[a] Slope from linear approximation of $\Delta R/R$ - p/p_o plots, in the form of Figure 3.12.

Table 3.2 Comparison of LODs of DNA-gold nanoparticle sensors with reported alkanethiol Au nanoparticle sensors

Vapor	LOD (ppm)			
	DNA (RH = 0%) [a]	DNA (RH = 50%) [a]	Octanethiol [30-31]	Hexanethiol [19]
Ethanol	475	266	4.9 to 49	242
Methanol	171	145	150	326
Toluene	211	32	0.082 to 2.3	48

[a] Defined as three times the baseline noise divided by sensitivity as appeared in Table 3.1.

3.2.4 DNA Length Effects

One typical feature of gold nanoparticle chemiresistive vapor sensors is the sensor's response scales linearly with capping molecule chain length [32]. To understand whether similar effect exists for DNA-functionalized gold nanoparticles used in chemiresistive sensors, a series of DNA oligomers of different lengths were tested. Figure 3.13 shows the response of poly A 10 mer and 50 mer towards toluene and water vapors. At $p/p_o = 0.50$, when vapors tested were organic vapors such as toluene, the sensors give a positive response. When the vapor tested is water vapor, the nanoparticle film is hydrated. For organic vapors, there is strong dependence of response on chain length, consistent with results in linear alkanethiol functionalized gold nanoparticles. Ionic conduction has dominated the sensor resistance decreases by at least two orders of magnitude, giving $\Delta R/R$ close to -1 for both sequences. In this case there is no response difference with respect to chain length.

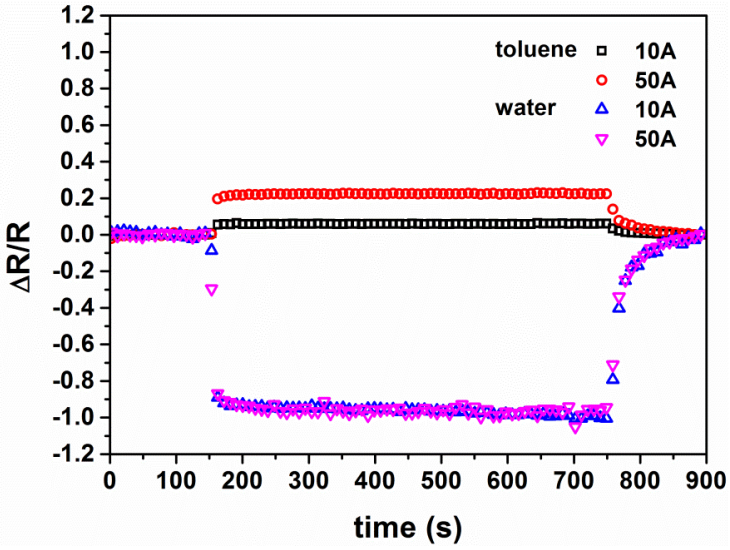

Figure 3.13 Real-time sensor response plot of 10-mer and 50-mer poly A functionalized gold nanoparticle chemiresistive sensors towards toluene and water at $p/p_o = 0.50$

For all vapors and all sequences tested, there is an approximate linear relationship between DNA chain length and response, as shown in Figure 3.14a. This shows that in the vapor-induced swelling regime, when bulkier ligands were used, larger volume of organic phase separating individual nanoparticles provides more adsorption sites. Therefore when there is more adsorption volume for organic vapors, the effect of tunneling distance on electron hopping current through the nanocomposite material is larger, and larger resistive response is recorded.

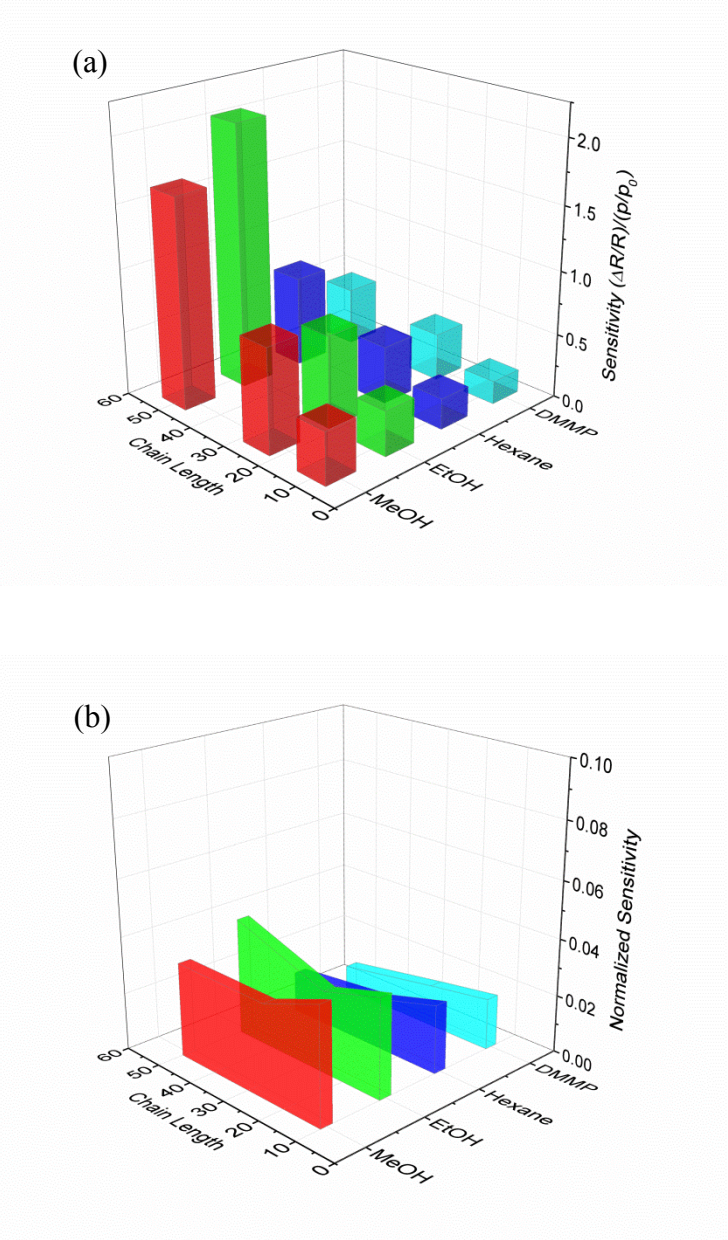

Figure 3.14 (a) Sensitivity of poly A DNA functionalized gold nanoparticle chemiresistive vapor sensors towards 4 vapors in the concentration range $p/p_o = 0$ to 0.20. Sensitivity is defined as slope from linear approximation of $\Delta R/R$ - p/p_o plots; (b) Normalized sensitivity based on (a), defined as the ratio of sensitivity against ligand length.

A very interesting key advantage of gold nanoparticle chemiresistive sensors is its ability to enhance adsorption-related responses. A very similar type of adsorption-based sensor is the quartz crystal microbalance (QCM) sensors [33]. The change in frequency of the QCM crystal upon exposure to analyte is analogous to resistance change in the chemiresistors, but the signal scaling behavior was found to be different in a recent study involving gold nanoparticles functionalized with alkanethiol chains of different lengths. With a QCM crystal modified with alkanethiol-functionalized gold nanoparticles, the sensitivity shows no significant dependence on the alkanethiol chain length, but for gold nanoparticle chemiresistive sensors, sensitivity scales with chain length [32]. A simple explanation is the sensor response of QCM is inherently based on change of mass per unit mass, which is already normalized. As the total material volume fraction in the sensor increases, the adsorbed mass also increases, so the fractional change of resonance frequency remains the same. In other words, the response of QCM sensor is already normalized against the mass of sensitive material. But nanoparticulate chemiresistors are based on current measurement, which is an absolute quantity that depends on the amount of material present. As current change is not normalized against the material mass, an increase in mass increases the total current response. This observation suggests that the gold nanoparticle chemiresistive sensors could become more sensitive by using longer organic chains.

However, if the sensor response is normalized against the chain length, which is a representation of the amount of material present, the sensitivity of gold nanoparticle chemiresistive sensors also becomes invariant towards chain length. As illustrated in Figure 3.14b, the sensitivities of DNA-functionalized gold nanoparticle sensors normalized against chain length towards all organic vapors are nearly independent on chain length. Assuming that the average number of DNA chains attached to the gold nanoparticles is the same, this behavioral

similarity with respect to alkanethiol-functionalized gold nanoparticles suggests that the swelling mechanism is the dominant source of sensor response in the dry state.

3.2.5 Beyond Sequence Dependence – Comparing Loop and Linear DNAs

DNA functionalized gold nanoparticle chemiresistive sensors can show variation of response towards a certain vapor by variation of nucleobase composition. However, the notable differences in sensor response are not surprising whatsoever, considering that the materials in terms of DNA sequences are very different. The DNA base components of the 4 types of sensors we have fabricated are fundamentally different, giving rise to unequivocally different response patterns. The source of response differences is the same type of van der Waals and dipole interaction differences specific to each molecule, which is an existing property of alkanethiol-functionalized gold nanoparticles. While compositional differences of surface ligands is certainly the source of response difference in gold nanoparticle chemiresistive sensors, it is thought-provoking to consider DNA as a polymer having three-dimensional conformations. Interaction parameters with gas phase vapor molecules may not be determined solely by simple physical chemistry of small molecules. Secondary or even tertiary structures of DNA might be additional interaction parameters. Therefore, rather than using DNA chains having the maximum difference in composition, it might be interesting to use DNA chains having identical composition but only different sequences. It could be hypothesized that the two sequences, albeit having the same compositions in terms of nucleobase content, could give rise to different responses solely based on the order in which the nucleobases are assembled on the DNA strand.

In this study, two ss-DNA strands having identical components but different sequences were compared. Figure 3.15 shows the 2 DNA sequences. Sequence 1 has base sequence 5'-HS-C_6H_6-AAA AGG GGA AAA AAA ACC CCT TTT-3', and Sequence 2 has base sequence 5'-HS-C_6H_6-GAA TTA ACA AAC CAG ATA ACG ATG-3'. Both sequences have the same composition – 8A, 4T, 4G, and 4C, but by free energy calculations, sequence 1 has an all-A loop structure while sequence 2 retains a linear structure.

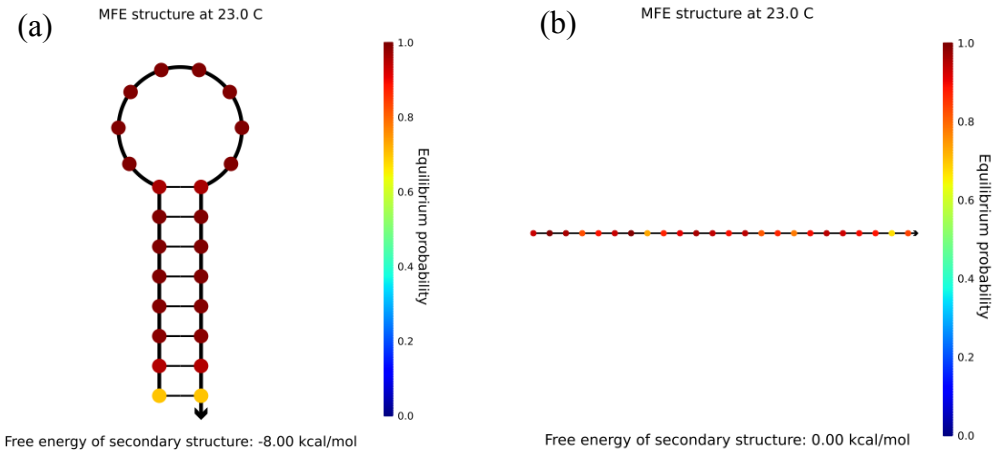

Figure 3.15 (a) Loop-structured Sequence 1; (b) linear-structured Sequence 2

DNA functionalized gold nanoparticle sensors with these two sequences and put them to concurrent tests for three vapors – hexane, toluene, and DMMP. The sensors were tested under a dry atmosphere, excluding interference from water vapor. Figure 3.16 depicts the sensor response to these three vapors at three different vapor pressures.

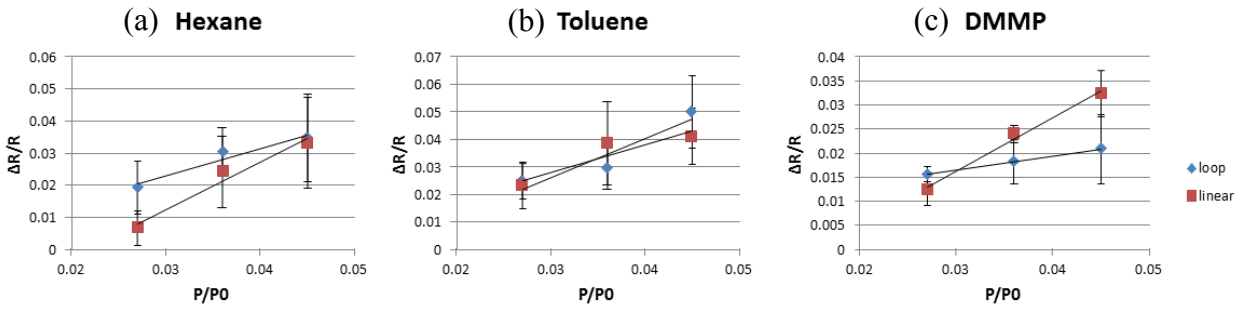

Figure 3.16 (a) Response of loop (sequence 1) and linear (sequence 2) towards hexane; (b) Response of loop (sequence 1) and linear (sequence 2) towards toluene; (c) Response of loop (sequence 1) and linear (sequence 2) towards DMMP

Table 3.3 shows the sensitivity and selectivity of loop (sequence 1) and linear (sequence 2) sensors towards hexane, toluene, and DMMP. Sensitivity of sensors is expressed as slope of sensor responses ($\Delta R/R$) against vapor concentrations (p/p_0). Selectivity is based on the ratios of sensitivity for both loop and linear sequences, using hexane as the reference.

Table 3.3 Sensitivity and selectivity of loop (sequence 1) and linear (sequence 2) sensors towards hexane, toluene, and DMMP

	Sensitivity ((ΔR/R)/(p/p0))			Selectivity (vapor/hexane)	
	hexane	toluene	DMMP	toluene/hexane	DMMP/hexane
loop (sequence 1)	0.85	1.41	0.28	1.65	0.34
linear (sequence 2)	1.47	0.99	1.10	0.68	0.75

Sensors with loop and linear DNA sequences were firstly compared based on selectivity of a common vapor, and secondly based on performance of each individual type of sensors. Selectivity-wise, the loop sequence is 2.44 times more selective for toluene than the linear structure, while the linear sequence is 2.21 times more selective for DMMP than the loop structure. More interestingly, if comparison is made horizontally across the table, the loop structure is 4.22 times more selective towards toluene compared to DMMP. On the other hand, the ratio of selectivity towards toluene and DMMP for linear structure is 0.91, which is close to 1. Considering that both loop (sequence 1) and linear (sequence 2) have exactly the same nucleobase composition but only differs in the order of nucleobase arrangement, the response pattern differences are likely to arise from interactions in excess of those solely determined by nucleobase contents. Given the fact that the 2 sequences are isomers, it can be postulated that the interaction differences might be from the three-dimensional conformations of the DNA sequences in space.

Table 3.4 is a list toluene-to-hexane selectivity ratios of organothiol gold nanoparticle chemiresistive sensors and DNA functionalized gold nanoparticle sensors. The choice of toluene and hexane is based on the fact that toluene is an aromatic molecule which could possibly offer π- π base stacking with nucleobases, while hexane is a linear alkane which is expected to swell an organic matrix in a most predictable fashion. Both molecules are relatively non-polar, therefore polarity-caused conductivity differences in sensors could be minimized.

For typical alkanethiols, the toluene/hexane selectivity ratio is about 1, which means that the sensors are not selective against the two vapors. The rare cases are 4-mercapotophenol, 4-

mercaptobenzoic acid, and 4-methylphenylthiol functionalized 3 nm nanoparticles, which give selectivity ratios close to 0.10. Given that this is a mixture of polar and non-polar ligands, particle core size could have played a role in determining their higher response to hexane than toluene. When the organic ligand volume is larger compared to the core, the sensors are generally not very selective against the two vapors. DNA-functionalized nanoparticles appear to be similar in this behavior, as even a 10-mer oligonucleotide is of greater volume to the typical organothiols. Typical selectivity of 10-mers, 25-mers, and 50-mers are all around 1. At RH = 50%, only Poly A 25-mer showing a greater selectivity at RH=50%, while other DNAs, poly T, poly C, and SEQ 02, have very close selectivity at about 1 – 2. The special high selectivity of poly A could be a combination of conformational preference of the DNA towards adsorption of toluene, as well as that the adenine base is special. Adenine is the only nucleobase that does not contain oxygen, and this may point to that the interaction between toluene and adenine is stronger than that for the other bases, thus favoring more adsorption.

For poly A DNA at RH = 0%, the selectivities are in the range 1 – 2 for 10-, 25-, and 50-mers. For poly T, poly C, and SEQ 02 25-mers, the selectivity at RH = 50% are all higher than the selectivity at RH = 0%. This behavior supports the suggestion that DNA has more conformational flexibility in a humid condition. The humid atmosphere is more favorable for base-stacking kind of adsorption, thus giving preference to toluene, but in the dry conditions, the adsorption favors hexane. In other words, nucleobases are more available for adsorptive interaction in a humid atmosphere. In the dry condition, poly A DNA functionalized gold nanoparticles behave most like long-chain alkanethiol gold nanoparticle chemiresististors in distinguishing toluene and hexane.

Overall, a humid atmosphere is shown to switch the vapor preferences of DNA gold nanoparticle chemiresistive sensors between toluene and hexane. The selectivity switch is most likely due to both conformational change which results in different functional groups interacting with vapor molecules and water-induced changes in interaction parameters of the two vapors. Secondly, DNA gold nanoparticles are more selective for toluene against hexane, as compared to many alkanethiol-functionalized gold nanoparticles. The selectivity preference is most likely due to preferable π-π base stacking with toluene molecules. As for the difference between loop and linear structures, the 2.4× difference in selectivity which is 1.65 for the loop compared to 0.68 for the linear, is very likely due to conformational differences. By forming a loop, the DNA molecule possibly prefers the adsorption of a ring-like molecule to a linear molecule, thus more adsorption of toluene than hexane.

The best toluene/hexane selectivity observed so far is 5.67 obtained with poly A 25-mer at RH = 50%, which is not dramatically enhanced as compared to the alkanethiol-functionalized gold nanoparticles in literature. Nevertheless, the results so far show preliminary evidences for a conformation-determined vapor adsorption, as well as purely sequence-dependent adsorption. It would be possible to control sorption behavior by tuning DNA sequences. There are two ways to achieve it: changing the nucleobase composition and through changing the nucleobase sequences within an identical composition.

Table 3.4 Toluene/Hexane selectivity of various gold nanoparticle chemiresistive vapor sensors. Sensitivities are expressed as sensor responses ($\Delta R/R$) against vapor concentrations (p/p_0).

Nanoparticle type	Toluene/Hexane Selectivity
Octanethiol, 4 nm [31]	1.16
11-mercaptoundecanoic acid, 5 nm [34]	0.94
1,9-nonanedithiolate, 5 nm [34]	0.91
11-mercaptoundecanoic acid, 2 nm [34]	0.78
1,9-nonanedithiolate, 2 nm [34]	1.01
4-mercaptophenol, 3 nm [35]	0.26
4-mercaptobenzoic acid, 3 nm [35]	0.10
4-aminophenylthiol, 6 nm [35]	1.76
4-methylphenylthiol, 3 nm [35]	0.10
Poly A, 10-mer (RH = 0%)	1.71
Poly A, 25-mer (RH = 0%)	1.18
Poly A, 50-mer (RH = 0%)	2.32
Poly T, 25-mer (RH = 0%)	0.83
Poly C, 25-mer (RH = 0%)	0.29
SEQ 02, 25-mer (RH = 0%)	0.17
Poly A, 25-mer (RH = 50%)	5.67
Poly T, 25-mer (RH = 50%)	1.11
Poly C, 25-mer (RH = 50%)	1.25
SEQ 02, 25-mer (RH = 50%)	1.59
LOOP (sequence 1) (RH = 0%)	1.65
LINEAR (sequence 2) (RH = 0%)	0.68

3.3 References

1. Ibañez, F. J.; Zamborini, F. P. Chemiresistive Sensing with Chemically Modified Metal and Alloy Nanoparticles. *Small* **2012,** *8* (2), 174-202.

2. Daniel, M.-C.; Astruc, D. Gold Nanoparticles: Assembly, Supramolecular Chemistry, Quantum-Size-Related Properties, and Applications toward Biology, Catalysis, and Nanotechnology. *Chemical Reviews* **2003,** *104* (1), 293-346.

3. Lin, Y.-W.; Liu, C.-W.; Chang, H.-T. DNA functionalized gold nanoparticles for bioanalysis. *Analytical Methods* **2009,** *1* (1), 14-24.

4. Peng, G.; Tisch, U.; Adams, O.; Hakim, M.; Shehada, N.; Broza, Y. Y.; Billan, S.; Abdah-Bortnyak, R.; Kuten, A.; Haick, H. Diagnosing lung cancer in exhaled breath using gold nanoparticles. *Nat Nano* **2009,** *4* (10), 669-673.

5. Pomogailo, A. D.; Kestelman, V. N. Principles and Mechanisms of Nanoparticle Stabilization by Polymers. In *Metallopolymer Nanocomposites*; Springer Berlin Heidelberg, 2005; Vol. 81, pp 65-113.

6. Storhoff, J. J.; Elghanian, R.; Mirkin, C. A.; Letsinger, R. L. Sequence-Dependent Stability of DNA-Modified Gold Nanoparticles. *Langmuir* **2002,** *18* (17), 6666-6670.

7. Herne, T. M.; Tarlov, M. J. Characterization of DNA probes immobilized on gold surfaces. *J Am Chem Soc* **1997,** *119* (38), 8916-8920.

8. Petrovykh, D. Y.; Kimura-Suda, H.; Whitman, L. J.; Tarlov, M. J. Quantitative analysis and characterization of DNA immobilized on gold. *J Am Chem Soc* **2003,** *125* (17), 5219-5226.

9. Petrovykh, D. Y.; Kimura-Suda, H.; Tarlov, M. J.; Whitman, L. J. Quantitative characterization of DNA films by X-ray photoelectron spectroscopy. *Langmuir* **2004,** *20* (2), 429-440.

10. Ray, S. G.; Cohen, H.; Naaman, R.; Rabin, Y. Where is the sodium in self-assembled monolayers of single-stranded DNA? *J Am Chem Soc* **2005,** *127* (49), 17138-17139.

11. Mourougou-Candoni, N.; Naud, C.; Thibaudau, F. Adsorption of thiolated oligonucleotides on gold surfaces: An atomic force microscopy study. *Langmuir* **2003,** *19* (3), 682-686.

12. Levicky, R.; Herne, T. M.; Tarlov, M. J.; Satija, S. K. Using self-assembly to control the structure of DNA monolayers on gold: A neutron reflectivity study. *J Am Chem Soc* **1998,** *120* (38), 9787-9792.

13. Zhang, R. Y.; Pang, D. W.; Zhang, Z. L.; Yan, J. W.; Yao, J. L.; Tian, Z. Q.; Mao, B. W.; Sun, S. G. Investigation of ordered ds-DNA monolayers on gold electrodes. *J Phys Chem B* **2002,** *106* (43), 11233-11239.

14. Yunker, P. J.; Still, T.; Lohr, M. A.; Yodh, A. G. Suppression of the coffee-ring effect by shape-dependent capillary interactions. *Nature* **2011,** *476* (7360), 308-311.

15. Joseph, Y.; Guse, B.; Vossmeyer, T.; Yasuda, A. Gold Nanoparticle/Organic Networks as Chemiresistor Coatings: The Effect of Film Morphology on Vapor Sensitivity. *The Journal of Physical Chemistry C* **2008,** *112* (32), 12507-12514.

16. Wohltjen, H.; Snow, A. W. Colloidal Metal−Insulator−Metal Ensemble Chemiresistor Sensor. *Analytical Chemistry* **1998,** *70* (14), 2856-2859.

17. Joseph, Y.; Guse, B.; Yasuda, A.; Vossmeyer, T. Chemiresistor coatings from Pt- and Au-nanoparticle/nonanedithiol films: sensitivity to gases and solvent vapors. *Sensors and Actuators B: Chemical* **2004,** *98* (2–3), 188-195.

18. Han Ha, D.; Nham, H.; Yoo, K.-H.; So, H.-m.; Lee, H.-Y.; Kawai, T. Humidity effects on the conductance of the assembly of DNA molecules. *Chemical Physics Letters* **2002,** *355* (5–6), 405-409.

19. Ibañez, F. J.; Zamborini, F. P. Chemiresistive Sensing of Volatile Organic Compounds with Films of Surfactant-Stabilized Gold and Gold−Silver Alloy Nanoparticles. *ACS Nano* **2008,** *2* (8), 1543-1552.

20. Pang, P.; Guo, Z.; Cai, Q. Humidity effect on the monolayer-protected gold nanoparticles coated chemiresistor sensor for VOCs analysis. *Talanta* **2005,** *65* (5), 1343-1348.

21. Segev-Bar, M.; Shuster, G.; Haick, H. Effect of Perforation on the Sensing Properties of Monolayer-Capped Metallic Nanoparticle Films. *The Journal of Physical Chemistry C* **2012,** *116* (29), 15361-15368.

22. Chalikian, T. V.; Sarvazyan, A. P.; Plum, G. E.; Breslauer, K. J. Influence of Base Composition, Base Sequence, and Duplex Structure on DNA Hydration - Apparent Molar Volumes and Apparent Molar Adiabatic Compressibilities of Synthetic and Natural DNA Duplexes at 25-Degrees-C. *Biochemistry-Us* **1994,** *33* (9), 2394-2401.

23. Tao, N. J.; Lindsay, S. M. Structure of DNA Hydration Shells Studied by Raman-Spectroscopy. *Biopolymers* **1989,** *28* (5), 1019-1030.

24. Berman, H. M.; Sowri, A.; Ginell, S.; Beveridge, D. A Systematic Study of Patterns of Hydration in Nucleic-Acids .1. Guanine and Cytosine. *J Biomol Struct Dyn* **1988,** *5* (5), 1101-1110.

25. Łukaszewicz, J. P.; Skompska, M. A novel carbon-based ionic conductor for humidity sensors. *Sensors and Actuators B: Chemical* **2006,** *113* (2), 970-977.

26. Zhou, Y.; Qin, Z.-Y.; Li, L.; Zhang, Y.; Wei, Y.-L.; Wang, L.-F.; Zhu, M.-F. Polyaniline/multi-walled carbon nanotube composites with core–shell structures as supercapacitor electrode materials. *Electrochimica Acta* **2010,** *55* (12), 3904-3908.

27. Mao, L.; Zhang, K.; On Chan, H. S.; Wu, J. Surfactant-stabilized graphene/polyaniline nanofiber composites for high performance supercapacitor electrode. *Journal of Materials Chemistry* **2012,** *22* (1), 80-85.

28. Zellers, E. T.; Han, M. Effects of Temperature and Humidity on the Performance of Polymer-Coated Surface Acoustic Wave Vapor Sensor Arrays. *Analytical Chemistry* **1996,** *68* (14), 2409-2418.

29. Han, L.; Daniel, D. R.; Maye, M. M.; Zhong, C. J. Core-shell nanostructured nanoparticle films as chemically sensitive interfaces. *Analytical Chemistry* **2001,** *73* (18), 4441-4449.

30. Guo, J. L.; Pang, P. F.; Cai, Q. Y. Effect of trace residual ionic impurities on the response of chemiresistor sensors with dithiol-linked monolayer-protected gold (nano)clusters as sensing interfaces. *Sensors and Actuators B-Chemical* **2007,** *120* (2), 521-528.

31. Steinecker, W. H.; Rowe, M. P.; Zellers, E. T. Model of Vapor-Induced Resistivity Changes in Gold−Thiolate Monolayer-Protected Nanoparticle Sensor Films. *Analytical Chemistry* **2007,** *79* (13), 4977-4986.

32. García-Berríos, E.; Gao, T.; Woodka, M. D.; Maldonado, S.; Brunschwig, B. S.; Ellsworth, M. W.; Lewis, N. S. Response versus Chain Length of Alkanethiol-Capped Au Nanoparticle Chemiresistive Chemical Vapor Sensors. *The Journal of Physical Chemistry C* **2010,** *114* (50), 21914-21920.

33. Sauerbrey, G. Verwendung von Schwingquarzen zur Wägung dünner Schichten und zur Mikrowägung. *Z. Physik* **1959,** *155* (2), 206-222.

34. Han, L.; Daniel, D. R.; Maye, M. M.; Zhong, C.-J. Core−Shell Nanostructured Nanoparticle Films as Chemically Sensitive Interfaces. *Analytical Chemistry* **2001,** *73* (18), 4441-4449.

35. Evans, S. D.; Johnson, S. R.; Cheng, Y. L.; Shen, T. Vapour sensing using hybrid organic-inorganic nanostructured materials. *Journal of Materials Chemistry* **2000,** *10* (1), 183-188.

Chapter 4

CONCLUSIONS AND FUTURE WORK

4.1 Summary and Conclusions

DNA-functionalized gold nanoparticles were used as a novel material to fabricate the nanocomposite films in chemiresistive vapor sensors. This pioneering work in characterization and sensing studies with DNA-functionalized gold nanoparticles revealed characteristics of this material most relevant to sensing applications. Some properties are very similar to small molecule organithiol functionalized gold nanoparticles, while others are very different.

To all the organic vapors tested, DNA functionalized gold nanoparticle chemiresistive sensors show an increase in resistance with increasing vapor concentration. This behavior is consistent with a swelling-dominated response mechanism agreed upon by most literature which treated the sensor material as a multitude of tunnel junctions. Even for water vapor, an increase in sensor resistance is observed for concentration up to $p/p_o = 0.4$. Sequence-dependent response patterns were observed, which could possibly be further analyzed by chemometric algorithms to allow pattern recognition and vapor identification. With a large number of possible DNA sequences used, the vapor differentiation capability of chemiresistive sensor arrays could be dramatically enhanced. This is the most encouraging aspect of DNA-based sensor arrays for future applications. Additional studies into DNA lengths indicated that the ligand length effect on chemiresistive sensing is similar to that for organothiol-functionalized gold nanoparticles. This behavior is consistent with the electron hopping mechanism.

Interestingly, DNA-functionalized gold nanoparticle sensors are highly sensitive to water sorption, displaying a dichotomous behavior. At low relative humidity (up to 40%), sensors

behave similarly to organothiol-functionalized gold nanoparticle sensors that respond to vapor partitioning and film swelling. At higher humidity (40% to 100%), sensors behave increasingly like a polyelectrolyte with ionic conduction contributions to the electrical response. As the film conduction mechanism changes dramatically, sensor responses to organic vapors under a humid condition also reverse and increase. The sensing of 5 vapors with 4 DNA oligomer sequences was studied at different relative humidity values and sequence dependent response patterns were also observed. The findings suggest that DNA-functionalized gold nanoparticle chemiresistors are comparable to alkanethiol-gold nanoparticle chemiresistive vapor sensors in terms of sensitivity and LOD. The high sensitivity to humidity indicates that careful control of water content is needed to distinguish analytes. Overall, the studies so far qualify gold nanoparticles functionalized with non-specific DNA as a useful new material for chemiresistive vapor sensing arrays.

While cost and complexity likely do not justify the use of random DNA as a weakly specific sensing material, understanding effects such as base sequence and sensing conditions will be necessary to design improved sensors that use aptamers for high specificity. In a dedicated study to test this possibility, two DNA sequences with identical compositions but only differ in nucleobase ordering within the chains, were concurrently tested. The selectivity difference in sensor responses to toluene, hexane, and DMMP serves as the first piece of evidence that using DNA allows for engineered selectivity. Continued study is needed to build the foundation for high specificity vapor sensing with DNA materials.

4.2 Ongoing and Future Work

Studying DNA-functionalized gold nanoparticles in chemiresistive vapor sensors engendered good understanding of the behaviors and capabilities of these new sensing materials. It advanced the field of integrating biomolecules with electronic systems and opens up many new opportunities. In the meantime, it revealed some limitations of nanoparticle-based chemiresistive sensing technology. Future work would be focused on continued effort in advancing the involvement of biomolecules in sensing, downscaling the sensors to even smaller sizes, and improving manufacturing technologies. These approaches share a common greater goal of achieving new frontiers in the field of portable chemiresistive sensing with an emphasis on biomolecule-based chemiresistive sensing.

4.2.1 Scaling Effect on Sensor Response Rate

Sensing miniaturization gives several practical advantages. It allows a denser array of sensors to be packed within a small volume, which allow more reliable analyte identification. Beyond this, it also promises enhanced portability, low electric power consumption, and greater networking capability. One attractive technology is the integration of sensors systems with smartphones for health monitoring. Recently, smartphone-based sensor systems have seen rapidly development, with the advent of pluggable sensors for blood glucose [1], sweat pH [2] and blood cholesterol [3]. The integration of hand-held devices with vapor sensors would provide an attractive way of health self-monitoring based on breath testing, air quality evaluation, and food testing. The possibility of integrating organothiol-functionalized gold nanoparticles and DNA-functionalized gold nanoparticles with hand-held devices improves the accessibility of these technologies, therefore creating broader benefits to the average person.

Preliminary downscaling studies were reported by Ancona et. al. [4] with the conclusion that the absolute sensitivity of the devices remains constant upon geometric scaling, but the signal-to-noise ratio increases. Despite the degradation in sensor performances, the authors are supportive for chemiresistive sensors of reduced size after weighing the benefits against the drawbacks. An important result of downscaling the devices is the enormous decrease in total sensor adsorption sites for vapor analytes. Therefore, sensors would reach equilibrium with the headspace faster on a purely kinetic basis. Sensor response rates would be expected to increase when the total number of nanoparticles decreases. It would be the next study to show this effect with the aid of a sensor testing system that allows more precise timing.

4.2.1.1 DMAP-Functionalized Gold Nanoparticles

In a model system, 4-dimethylaminopyridine (DMAP) functionalized gold nanoparticles were assembled in sub 100 nm gap devices and their performances were evaluated against the micron-sized devices. DMAP functionalized gold nanoparticles were prepared using the Brust method [5] followed by the phase transfer procedure developed by Gittins et. al. [6]. 70 ml of 2% $HAuCl_4 \cdot 3H_2O$ was added to a stirred solution of 8.752 g of TOAB in 320 ml of toluene. Stirring was continued for 10 min, and 1.892 g of solid $NaBH_4$ was added to reduce Au^{3+} to elemental gold. After 2 h, the lower aqueous phase was removed and the toluene phase was washed with 200 ml of 0.1 M H_2SO_4 followed by 200 ml of 1 M Na_2CO_3, and finally with deionized water. To switch to DMAP ligand, an aqueous solution (50 ml) of 0.6446 g DMAP was added to the as-prepared nanoparticles in toluene. Phase transfer from toluene to aqueous phase occurred spontaneously. The resulting DMAP gold nanoparticle solution was concentrated under a gentle stream of nitrogen at room temperature to reach a 1% w/v concentration.

This study would provide the direction for future efforts on whether to go to single nanogap devices when technology allows. Surface characterization of DMAP functionalized gold nanoparticles was not necessary as only a single material was used. Its surface composition is not of primary interest to this study and most studies excluded a discussion on functionalization efficiency of small-molecule functionalized gold nanoparticles. Furthermore, DMAP functionalized gold nanoparticles have been well-characterized in both film and powder forms [7-8]. Ligand stability has been established by these studies. DMAP-functionalized gold nanoparticles have an average diameter of 5 ~ 6 nm with occasional particles with sizes larger than 10 nm.

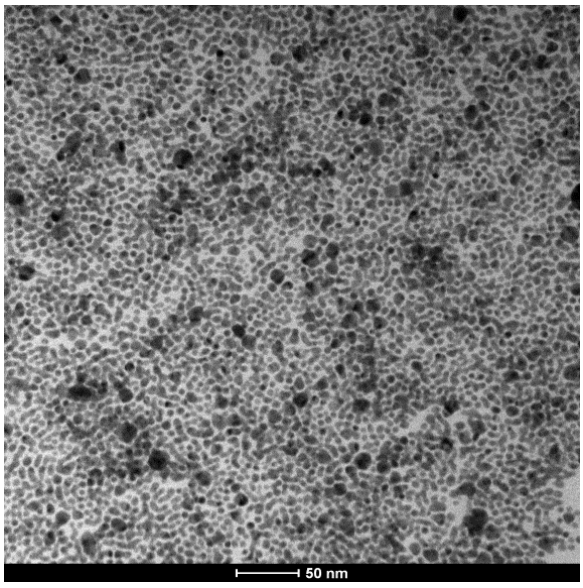

Figure 4.1 5 ~ 6 nm DMAP-functionalized gold nanoparticles

4.2.1.2 Deposition of DMAP Functionalized Nanoparticles on 20 µm Circular Electrodes

The deposition of DMAP functionalized gold nanoparticles was very similar to DNA functionalized gold nanoparticles. 4 µl of gold nanoparticle concentrate was deposited on each

sensor area. The droplet readily wets the electrode areas, and was evaporated under a dry air atmosphere at room temperature. DC resistances measured in air have a resistivity in the range of a few to 50 kΩ. Microstructural features of DMAP-functionalized gold nanoparticles were similar to DNA-functionalized gold nanoparticles.

4.2.1.3 Deposition of DMAP Functionalized Nanoparticles on 50 nm Nanogap Electrodes

50 nm gap line-spacing devices were fabricated through 2 steps. 4-inch silicon wafer with 300 nm of thermally grown oxide was also used as the substrate. First, line patterns of palladium electrodes were fabricated using photolithograph, electron-beam evaporation and lift-off processes. Afterwards, tips were fabricated using electron-beam lithography, electron-beam evaporation, and lift-off processes. This second process produces the sharp nanometer-sized tips, which would be used to study electron transport through gold nanoparticles in sub-50 nm gaps. (Figure 4.2)

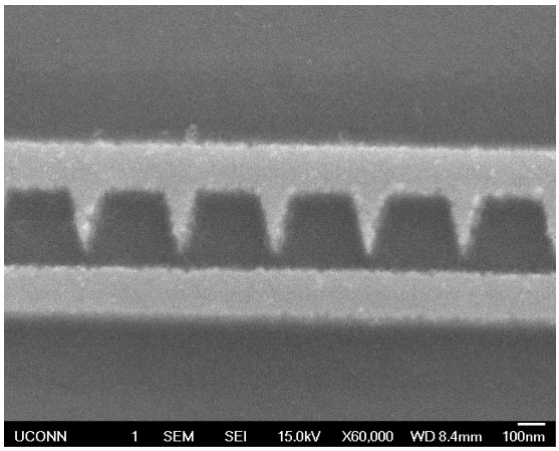

Figure 4.2 Parallel Pd electrodes with a spacing of 250 nm. The spacing at tips is 50 nm.

While trying to decrease the size to sub 100 nm scales, dielectrophoresis plays a very useful role in assembling nanoparticles in a designated area. DMAP functionalized gold nanoparticles solution was further diluted in deionized water to a concentration of 0.02% w/v. The assembly of DMAP functionalized nanoparticles were aided by dielectrophoresis, similar to literature-described method [9]. An AC electric output of 1 MHz, with sinusoidal waveform of peak-to-peak voltage (V_{pp}) of 1 V, was supplied by an Agilent 33220A function generator to the 50 nm nanogap devices. The two terminals were applied to each of the two electrodes, as shown in Figure 4.3. A 1 µl droplet of DMAP functionalized gold nanoparticle solution was carefully placed on the device surface, covering the pair of palladium electrodes which had the AC voltage applied. This configuration was maintained for 5 min and the nanoparticle solution was allowed to dry. After the completion of the dielectrophoresis assembly process, excess nanoparticle solution was blown off by a nitrogen stream.

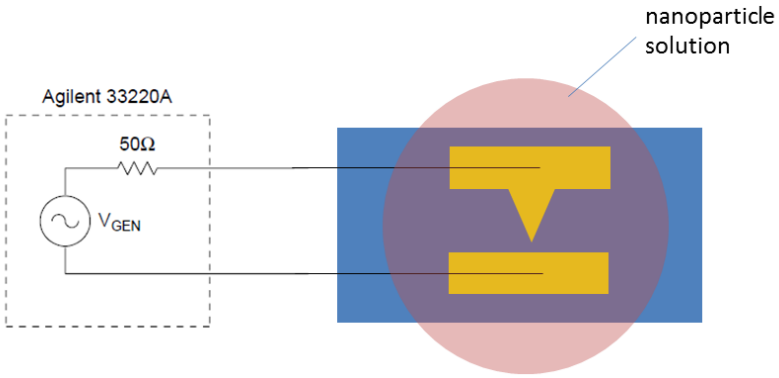

Figure 4.3 Schematics of dielectrophoretic nanoparticle assembly

4.2.1.4 Preliminary Results of Nanogap Devices

Analysis by SEM coupled with EDX provides the most direct evidence of nanoparticle assembly on the nanoscale. Figure 4.4(a) shows the changes of nanogap electrodes after deposition of DMAP-functionalized gold nanoparticles using dielectrophoresis. It is evident that high density of gold nanoparticles are assembled in between the line electrodes, both in the wider 250 nm gaps and the narrower 50 nm tip-to-line gaps. Gold nanoparticle assemblies appear as bright-colored patches. On the other hand, no gold nanoparticles were assembled at a distance more than a few hundred nanometers away from the line electrodes. Comparatively, Figure 4.4(b) shows a similar pair of line electrodes which were not connected to the high frequency AC field. Small clusters of DMAP-functionalized gold nanoparticles were seen everywhere on the substrate surface, probably as a result of adsorption. And there's no local concentration of nanoparticles anywhere on the electrode surface.

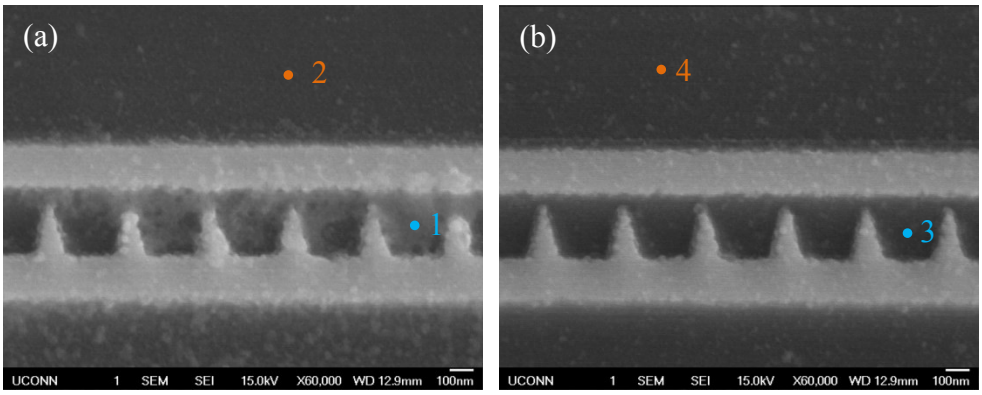

Figure 4.4 SEM images of (a) Nanogap electrode after dielectrophoresis. 1 MHz, 1 V_{pp} AC field was applied to the two line electrodes. Points 1 and 2 were analyzed by EDX and quantitative results were listed in Table 4.1. (b) Nanogap electrode immersed in dielectrophoresis solution but no AC field was applied to the two line electrodes. Points 3 and 4 were analyzed by EDX and quantitative results were listed in Table 4.1.

To further verify that the assembled materials in between the electrodes are gold nanoparticles, EDX was used to verify the chemical composition. Table 4.1 summarizes the chemical composition obtained by taking point-select EDX spectra on positions indicated in Figure 4.4. Not surprisingly, the device which has gone through dielectrophoresis had a 1.53% of Au, as compared to 0.21% for non-dielectrophoretic devices. Considering that EDX has a typical sampling depth of 1 μm, with the majority of the signals coming from the Si substrate, 1.53% Au on the nanogap dielectrophoretic sample is a significant indication of successful deposition of gold nanoparticles in the gap. SEM together with EDX proves that dielectrophoresis is assistive in directing local nanoparticle assembly, as compared to non-controlled adsorption of gold nanoparticles.

Table 4.1 Atomic percentages on selected spots in Figure 4.4

Atomic Percentages (%)	C	O	Si	Ti	Pd	Au
(1) Inside nanogap after dielectrophoresis	43.20	4.99	48.23	0.20	1.86	1.53
(2) Outside nanogap after dielectrophoresis	35.97	9.30	54.83	-	-	-
(3) Inside nanogap, control	43.54	7.82	48.06	-	0.38	0.21
(4) Outside nanogap, control	38.71	9.41	51.88	-	-	-

Figure 4.5 shows the I-V curves of a 20 μm device with poly A DNA-functionalized gold nanoparticles, a 20 μm device with DMAP-functionalized gold nanoparticles, and a 50 nm nanogap device with DMAP-functionalized gold nanoparticles, collected with a pure N_2 flow at

600 cm^3/min. The I-V curve of a 20 μm DNA-functionalized gold nanoparticle devices is included for comparative purposes. On the 20 μm devices, the I-V curves are both approximately linear and are ohmic type, regardless the materials deposited on it. However, the nanogap device shows a distinctive S-shaped curve.

The I-V curve differences could also be sufficiently explained by the percolation theory developed by Joseph et. al. and thoroughly explained in Chapter 3 [10]. The 20 μm devices in Figure 4.5a and Figure 4.5b are fabricated by drop-casting. The film nanoparticle films formed are of various thicknesses across the device surface, with certain areas covered by multiple layers of nanoparticles. Therefore a well-interconnected nanoparticle network dominates the electrical conduction and the I-V curves are both linear. DNA-functionalized nanoparticles have a larger resistance than DMAP-functionalized nanoparticles, primarily due to lower nanoparticle concentration used for drop-casting as well as larger space occupied by the polymeric DNA molecules as compared to small-molecule DMAP. The nanogap devices in Figure 3.4c were fabricated by dielectrophoresis trapping. As the nanoparticle solution used were diluted 10 times and excess nanoparticles were blown off after the deposition process, the amount of nanoparticles left over in the gaps were very small. The result of this small-number of nanoparticles being active conductors is that multiple incomplete percolation pathways were dominating the electron transport. Therefore, S-shaped curves are reminiscent of the presence of Coulomb blockade. It needs to be noted that to verify this effect, a range of temperatures should be used to show activated charge transport.

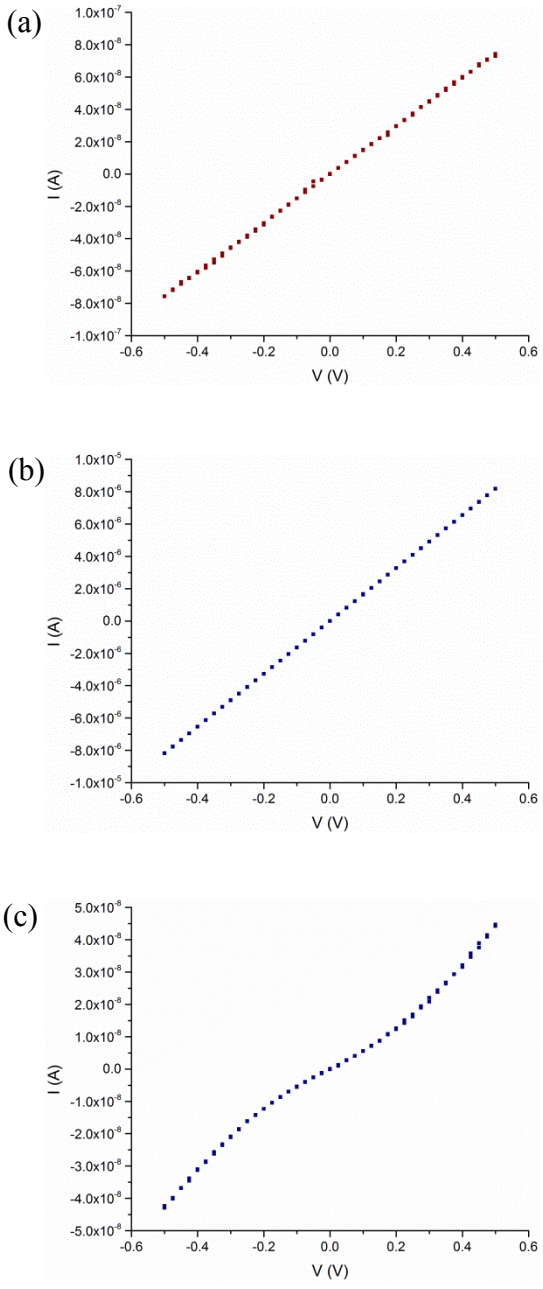

Figure 4.5 I-V curves of (a) a 20 μm device with poly A DNA-functionalized gold nanoparticles, (b) a 20 μm device with DMAP-functionalized gold nanoparticles, and (c) a 50 nm nanogap device with DMAP-functionalized gold nanoparticles**.**

4.2.2 Molecular Electronic Sensors

As first introduced in Chapter 1, the ultimate nanogap devices would be a single tunnel junction devices fully transform the current sensors into a molecular electronic device. While fixed single tunnel junction electrodes may forbid the sensing mechanisms which work by swelling, the system could be used for detecting additional analyte signatures through scanning tunneling spectroscopy (STS). Empty monolithic nanoscopic tunnel junctions produced using atomic layer deposition (ALD) successful identified bond information in acetic acid vapor molecules [11]. Bond information was represented as peaks in the second-derivative d^2I/dV^2 plots (Figure 4.6 a, b). Similarly, using a scanning tunneling microscope (STM) combined with a single in-gap nanoparticle, multiple organic vapors were identified by their Coulomb gap differences [12]. In the meantime, DNA-based molecular electronic devices have been extensively studied for fabrication techniques and charge transport (Figure 4.6 c, d) [13-14]. To go beyond vapor identification using only resistance-time information, a new type of sensor combining both resistance change and spectroscopic information could be developed.

A second very important feature is the ultimate rapid signaling that could be achieved with single-molecule devices. Nanogap devices in Section 4.2.1 is a way to improve the sensor response rate by decreasing the sensor volume by thousands of times. However, the sensing elements are still clusters of gold nanoparticles with a multi-layer structure. Although it is expected to improve the sensor response, the transport of vapor analytes would still go through a diffusion path through the sensor material, whose dimension is determined by the gap distance and the electrode thickness and estimated to be on the order of thousands of nm^3. Therefore, further downscaling of the devices could lead to another boost in response rate.

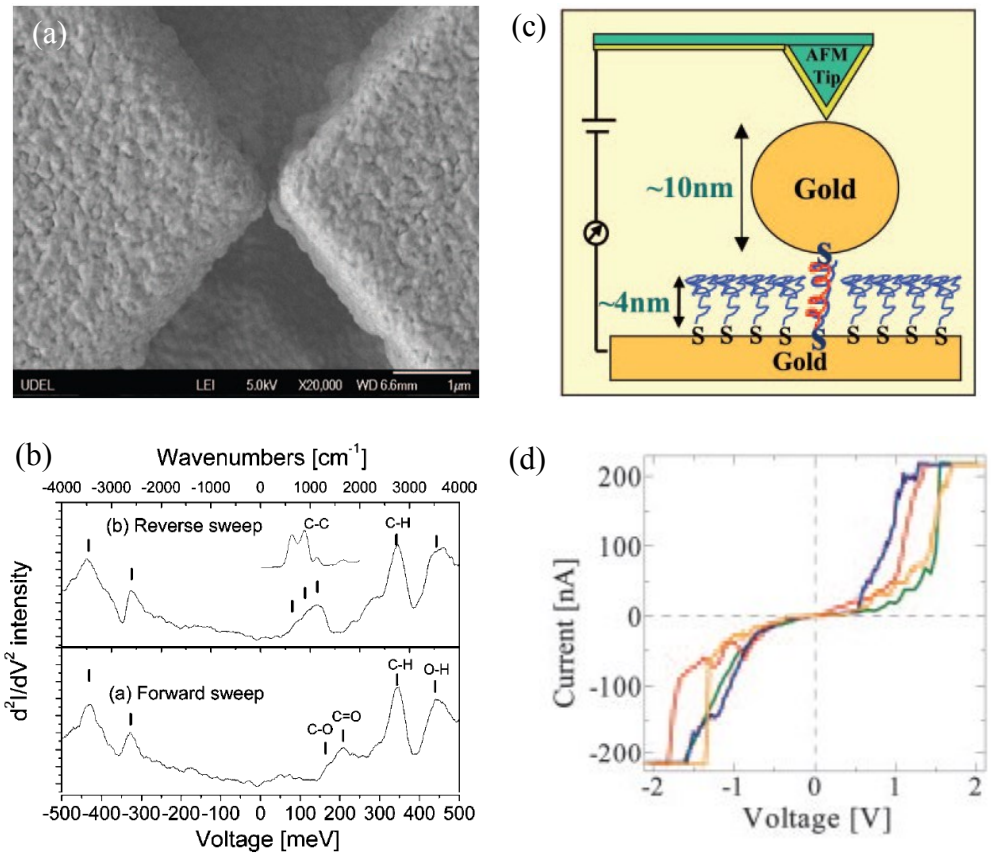

Figure 4.6 (a) ALD deposited tunnel junction and (b) the STS spectra obtained for acetic acid; (c) configuration for direct measurement through single DNA molecules and (d) the I-V curves obtained on such configuration

4.2.3 Fabrication Sophistication

A survey of current literature leads to a simple conclusion that current fabrication technology for gold nanoparticle chemiresistive vapor sensors has limited sophistication. In fact, this is a limitation that has not been overcome in this thesis as well. Commonly used methods

such as drop-casting, air brushing and dip-coating provide, to a best approximation, macroscopic control of nanoparticle film morphology. The films produced are usually of non-uniform thickness, and the variance in average thickness of a batch of samples is also large. Therefore, intra-batch variance of sensor response is large, and non-functioning sensors are frequently produced, either as a result of a short circuit or open circuit. These are some of the primary reasons to overcome before commercialization of gold nanoparticle chemiresistive vapor sensors for any kind of surface functionalization ligands.

Inkjet printing has been used as an alternative tool to deposit gold nanoparticles for chemiresistive sensing [8, 15-16]. By using an Autodrop printing system with a drop volume as small as 180 pl, gold nanoparticle films of minute sizes can be deposited. Although inkjet printing alone were not shown to improve film morphologies, it provided a useful way of defining gold nanoparticle patterns at precise locations on the substrate. Inkjet printing could be adapted to deposition of DNA-functionalized gold nanoparticles, improving the precision of nanoparticle film location and thickness uniformity.

Minimizing coffee-ring effect is a central theme in solution deposition of colloid particles. The coffee-ring structure is due to pinning of the contact line as the solvent evaporates and a faster solvent loss from the edge of the deposited droplet. A few methods have been used to overcome this effect, for example, by using a non-sticky Teflon substrate, by confining the solvent evaporation space [17], or by tweaking solvent composition thus its evaporative properties [18]. The solvent property method has been successfully used to produce more uniform-thickness gold nanoparticle films [19]. It is therefore useful to attempt similar kinds of parameter control to produce higher quality, more uniform nanoparticle films, which would

improve the reproducibility of nanoparticle-based chemiresistive sensing devices. However, for nanogap devices, inkjet droplets may still be too big for accurate placement with nanogaps, and dielectrophoresis remains the most viable option for depositing small amount of nanoparticles within nanogaps.

4.2.4 Chemometric Analysis for DNA Functionalized Gold Nanoparticle Sensor Arrays

Chemometric analysis using tools such as principal component analysis (PCA) and linear discriminant analysis (LDA) are common techniques for array-based analyte identification. In principle, when highly specific analyte-sensor interactions are not available, DNA-functionalized gold nanoparticle chemiresistive sensor arrays could be used with chemometric analysis in the same fashion. Figure 4.7 shows a preliminary PCA plots using the raw data from Chapter 3. The PCA algorithm was implemented using R Programming Language in RStudio software package. Using three sensors for each DNA sequence, the sensor array was able to distinguish the vapors tested with performance comparable to a sensor array based on small molecule organothiol-functionalized gold nanoparticles [20] and carbon nanotubes [21]. However, the significance of the vapor distinguishing power needs to be further proved with a larger number of DNA sequences. The 4 sequences selected for the study represented the some of the maximum differences that could be incorporated in the DNA sequence, for example, an all-A compared with all-T. Therefore future experiments need to be performed to verify the robustness of a sensor arrays with a larger number of members. To improve the sensor array performance, it might be necessary to use artificial nucleobases in the DNA sequences to further engineering the sequence-to-sequence variation in adsorptive properties [22]. As already noted, fluorescence-based DNA arrays in vapor recognition was studied, yielding encouraging results

[23]. Further sensor array development with DNA-functionalized gold nanoparticles could be promising.

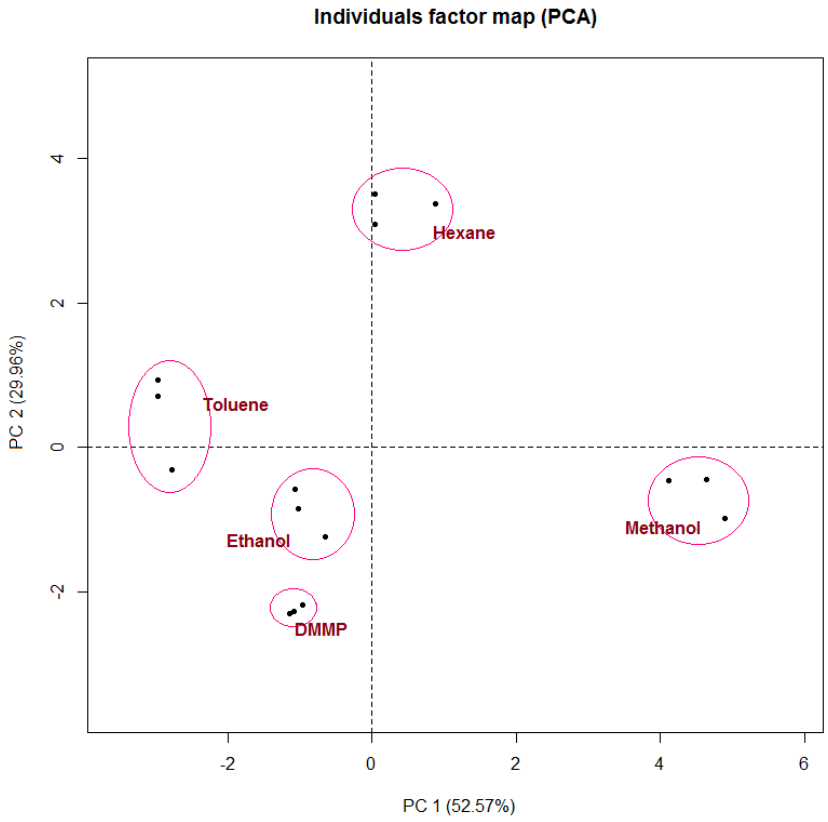

Figure 4.7 PCA plot of an array of 4 DNA sequences in distinguishing 5 vapors tested in Chapter 2

4.2.5 Charge Transport Mechanisms of Nanocomposite Films

Although the field of functionalized gold nanoparticle chemiresistive vapor sensors has developed tremendously since its inception in 1998, the fundamental understanding of charge transport in the nanocomposite film structure is still incomplete. As mentioned in Chapter 1, two sensor response mechanisms were proposed – film swelling and dielectric constant change. To

date, no undisputed conclusions have been made on which mechanism is dominant. Although for simple covalent alkanethiol molecules it is widely accepted that swelling is dominant over dielectric constant effects [10, 24-25], a conclusion has not been made for more complex ionic ligand films which comprise charged small molecules or polyelectrolytes. Even for simple alkanethiol functionalized gold nanoparticles, the quantitative relative weightage of two sensing mechanisms remains elusive [26]. One possible way to decouple the two sensing mechanism is to reproduce the sensing conditions using immobile electrodes for electron tunneling. This design would preclude swelling effect and allows the dielectric effect to be independently probed.

For charged molecules at higher relative humidities, charge transport turns ionic. In this case, mobile ions play a role in charge transport. The nanocomposite film no longer assumes an electron hopping model, and there would be charge transport between metal nanoparticles and polymer matrix across an electrode-electrolyte interface. In this case, interfacial effects need to be considered when dealing with metal-organic nanocomposite materials [27]. A completely new model needs to be built to account for the material behavior under humid conditions.

4.2.6 Other Biomolecules

4.2.6.1 More DNA Structures

Biological systems present a vast library of molecules of vast complexity. Inspired by this, aptamer-based bioelectronics is a very popular concept in liquid-phase sensing in recent years [28-29]. Studies presented in Chapters 1 – 3 utilized some of the most distinct DNA sequences to produce nanoparticle-based chemiresistive sensors. The results were promising in that firstly distinctive DNA sequences give widely different response patterns, and secondly

DNA sequences of identical composition and different nucleobase orders produced varying selectivity. Therefore, expanded investigation of DNA sequences including some with known three-dimensional structures could be one step closer to molecular recognition.

Although vapor phase aptamer was tested for riboflavin in one study [30], its response profile as well as selectivity is not conclusive. To date, there is no report of a reliable vapor phase aptamer. In the absence of purposeful design of three-dimensional structures reported to date, all studies so far involving apparently random DNA sequences [23, 31-32]. To further the field, it would be of interest to first investigate the effect known three-dimensional structures on vapor sensitivity. An immediate step after the loop DNA study in Chapter 3 is to use more DNA sequences with identical compositions. For example, for three block sequences of a certain number of nucleobases in length represented by A, B, C, there are a total of 6 different combinations of sequences, displayed in Figure 4.8.

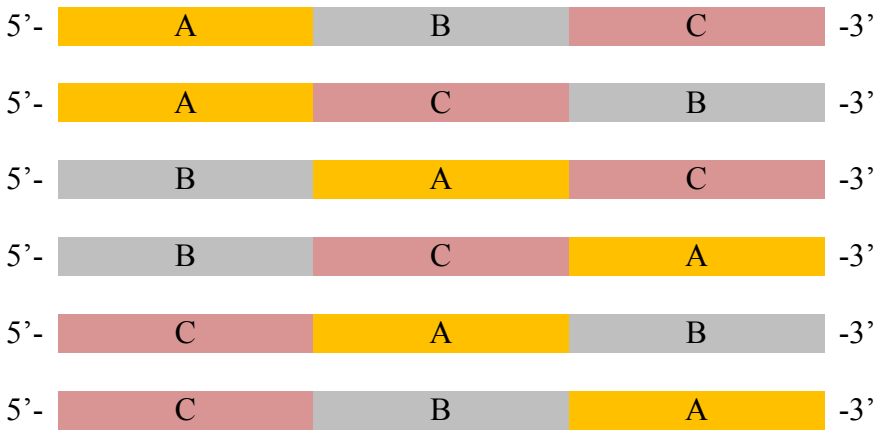

Figure 4.8 6 different sequences deriving from the same three block sequences – A, B, and C

All 6 sequences are isomers, but they could show very different adsorbing properties. Differences in adsorption properties could depend on bases which are relatively exposed, and the possible three-dimensional structural differences among the 6 sequences. It would be the first study to show the differences between these sequences towards common organic vapors.

Special sequence characteristics or defined symmetry elements are required to form alternative structures such cruciform structures, intramolecular triplexes, quadruplex DNA, slipped-strand DNA, parallel-stranded DNA, and unpaired DNA structures (Figure 4.9) [33].

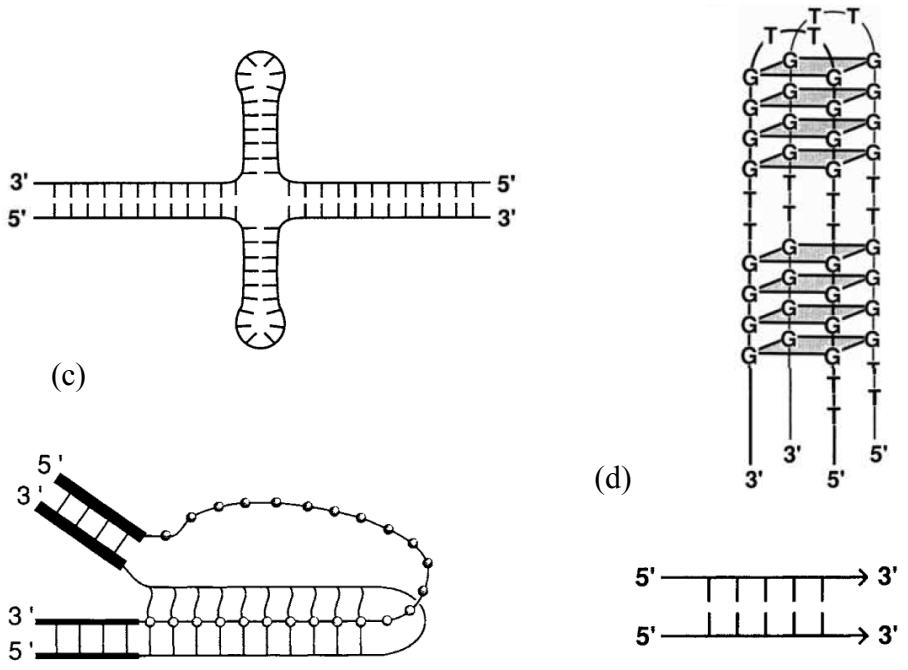

Figure 4.9 Examples of three-dimensional DNA conformations determined by base sequence. (a) cruciform structure; (b) quadruplex structure; (c) triplex structure; (d) parallel-stranded DNA [33]

Testing these more complex structures in addition to single loop structure represents more opportunities at achieving highly specific analyte-material interaction. Future experiments would be targeted at testing vapor phase sensitivity with naturally occurring and specially designed more complex structures. Compared with linear random structures, complex structures would likely show different adsorption preferences, and therefore different selectivity. Beyond naturally occurring complex structures, complementary base-pairing allows for the creation of many synthetic nanostructures in a technique termed "DNA origami" [34]. One important feature of this study is that the complex DNA structures are stable upon drying and exposing to vacuum conditions. The stability of these DNA nanostructures in dry conditions is an encouraging fact for potential application of DNA nanostructures for vapor sensing. In addition, the freedom of three dimensional structure designs allows the possibility of specific detection of vapor targets are hard to distinguish by conventional means. These studies would assist in understanding the effect of DNA-vapor interactions and crafting highly specific vapor phase molecular recognition.

4.2.6.2 Peptide-Based Vapor Sensors

Another class of biomolecules that is of interest to sensing is proteins. Although known to be less stable than aptamers, proteins are more complex and hence present even greater opportunity for exploring highly specific analyte-sensor interaction. While DNA sequences have only 4 types of nucleobases as building blocks, proteins have 20 common amino acids. Besides, many of the successful selective sensing technologies are based on proteins, notably enzymatic blood glucose test strips. While under the right physiological conditions, enzymes are known to have high molecular recognition capability. The use of proteinaceous materials in sensing represents many opportunities in highly selective sensing. More recently, single molecule

protein transistors have recently been demonstrated by inserting an immunoglobulin G into a tunnel junction device [35]. Further down the road, it is foreseeable that proteins could be used in addition to DNA as molecular recognition elements. Compared to DNA, proteins have more diverse three-dimensional structures with more well-known ligand-receptor systems, but proteins have 20 different types of building blocks, are more complex, and are less stable. Using proteins as chemiresistive vapor sensing elements could possibly improve sensor selectivity towards desired targets, but it is more challenging in terms of fabrication technologies and device stability.

In a months-old study, peptide-functionalized gold nanoparticles were used to test the capability of a new sensing material [36]. While specific selectivity towards a certain target vapor was not analyzed, the sensor displayed pattern recognition capabilities based on multivariate transducers. Along with DNA-functionalized gold nanoparticle sensors developed in this work, it heralds the field of using biomolecules in electronic vapor detection. While vapor sensing capabilities of proteinaceous and DNA materials have been both successfully demonstrated, it will be the next step to engineer highly selective sensing materials based on molecular recognition principles using either protein, DNA, or any biomolecules that confer ligand-receptor binding properties.

4.3 References

1. Tran, J.; Tran, R.; White, J. R. Smartphone-Based Glucose Monitors and Applications in the Management of Diabetes: An Overview of 10 Salient "Apps" and a Novel Smartphone-Connected Blood Glucose Monitor. *Clinical Diabetes* **2012,** *30* (4), 173-178.

2. Oncescu, V.; O'Dell, D.; Erickson, D. Smartphone based health accessory for colorimetric detection of biomarkers in sweat and saliva. *Lab on a Chip* **2013,** *13* (16), 3232-3238.

3. Oncescu, V.; Mancuso, M.; Erickson, D. Cholesterol testing on a smartphone. *Lab on a Chip* **2014**.

4. Ancona, M. G.; Snow, A. W.; Foos, E. E.; Kruppa, W.; Bass, R. Scaling Properties of Gold Nanocluster Chemiresistor Sensors. *Sensors Journal, IEEE* **2006,** *6* (6), 1403-1414.

5. Brust, M.; Walker, M.; Bethell, D.; Schiffrin, D. J.; Whyman, R. Synthesis of thiol-derivatised gold nanoparticles in a two-phase Liquid-Liquid system. *Journal of the Chemical Society, Chemical Communications* **1994,** (7), 801-802.

6. Gittins, D. I.; Caruso, F. Spontaneous Phase Transfer of Nanoparticulate Metals from Organic to Aqueous Media. *Angewandte Chemie International Edition* **2001,** *40* (16), 3001-3004.

7. Yu, A.; Liang, Z.; Cho, J.; Caruso, F. Nanostructured Electrochemical Sensor Based on Dense Gold Nanoparticle Films. *Nano Letters* **2003,** *3* (9), 1203-1207.

8. Raguse, B.; Chow, E.; Barton, C. S.; Wieczorek, L. Gold Nanoparticle Chemiresistor Sensors: Direct Sensing of Organics in Aqueous Electrolyte Solution. *Analytical Chemistry* **2007,** *79* (19), 7333-7339.

9. Kumar, S.; Yoon, S.-H.; Kim, G.-H. Bridging the nanogap electrodes with gold nanoparticles using dielectrophoresis technique. *Current Applied Physics* **2009,** *9* (1), 101-103.

10. Joseph, Y.; Guse, B.; Vossmeyer, T.; Yasuda, A. Gold Nanoparticle/Organic Networks as Chemiresistor Coatings: The Effect of Film Morphology on Vapor Sensitivity. *The Journal of Physical Chemistry C* **2008,** *112* (32), 12507-12514.

11. Gupta, R.; Appelbaum, I.; Willis, B. G. Reversible Molecular Adsorption and Detection Using Inelastic Electron Tunneling Spectroscopy in Monolithic Nanoscopic Tunnel Junctions. *The Journal of Physical Chemistry C* **2009,** *113* (9), 3874-3880.

12. Xu, L.-P.; Chen, S. Scanning tunneling spectroscopy of gold nanoparticles: Influences of volatile organic vapors and particle core dimensions. *Chemical Physics Letters* **2009,** *468* (4–6), 222-226.

13. Porath, D.; Cuniberti, G.; Felice, R. Charge Transport in DNA-Based Devices. In *Long-Range Charge Transfer in DNA II*, Schuster, G. B., Ed.; Springer Berlin Heidelberg, 2004; Vol. 237, pp 183-228.

14. Porath, D.; Bezryadin, A.; de Vries, S.; Dekker, C. Direct measurement of electrical transport through DNA molecules. *Nature* **2000,** *403* (6770), 635-638.

15. Cooper, J. S.; Raguse, B.; Chow, E.; Hubble, L.; Müller, K.-H.; Wieczorek, L. Gold Nanoparticle Chemiresistor Sensor Array that Differentiates between Hydrocarbon Fuels Dissolved in Artificial Seawater. *Analytical Chemistry* **2010,** *82* (9), 3788-3795.

16. Raguse, B.; Barton, C. S.; Müller, K.-H.; Chow, E.; Wieczorek, L. Gold Nanoparticle Chemiresistor Sensors in Aqueous Solution: Comparison of Hydrophobic and Hydrophilic Nanoparticle Films. *The Journal of Physical Chemistry C* **2009,** *113* (34), 15390-15397.

17. Deegan, R. D.; Bakajin, O.; Dupont, T. F.; Huber, G.; Nagel, S. R.; Witten, T. A. Contact line deposits in an evaporating drop. *Physical Review E* **2000,** *62* (1), 756-765.

18. Tekin, E.; de Gans, B.-J.; Schubert, U. S. Ink-jet printing of polymers - from single dots to thin film libraries. *Journal of Materials Chemistry* **2004,** *14* (17), 2627-2632.

19. Chow, E.; Herrmann, J.; Barton, C. S.; Raguse, B.; Wieczorek, L. Inkjet-printed gold nanoparticle chemiresistors: Influence of film morphology and ionic strength on the detection of organics dissolved in aqueous solution. *Analytica Chimica Acta* **2009,** *632* (1), 135-142.

20. Wang, L.; Luo, J.; Yin, J.; Zhang, H.; Wu, J.; Shi, X.; Crew, E.; Xu, Z.; Rendeng, Q.; Lu, S.; Poliks, M.; Sammakia, B.; Zhong, C.-J. Flexible chemiresistor sensors: thin film assemblies of nanoparticles on a polyethylene terephthalate substrate. *Journal of Materials Chemistry* **2010,** *20* (5), 907-915.

21. Zilberman, Y.; Tisch, U.; Shuster, G.; Pisula, W.; Feng, X.; Müllen, K.; Haick, H. Carbon Nanotube/Hexa-peri-hexabenzocoronene Bilayers for Discrimination Between Nonpolar Volatile Organic Compounds of Cancer and Humid Atmospheres. *Advanced Materials* **2010,** *22* (38), 4317-4320.

22. Samain, F.; Ghosh, S.; Teo, Y. N.; Kool, E. T. Polyfluorophores on a DNA Backbone: Sensors of Small Molecules in the Vapor Phase. *Angewandte Chemie International Edition* **2010,** *49* (39), 7025-7029.

23. White, J.; Truesdell, K.; Williams, L. B.; AtKisson, M. S.; Kauer, J. S. Solid-State, Dye-Labeled DNA Detects Volatile Compounds in the Vapor Phase. *PLoS Biol* **2008,** *6* (1), e9.

24. Olichwer, N.; Leib, E. W.; Halfar, A. H.; Petrov, A.; Vossmeyer, T. Cross-Linked Gold Nanoparticles on Polyethylene: Resistive Responses to Tensile Strain and Vapors. *ACS Applied Materials & Interfaces* **2012,** *4* (11), 6151-6161.

25. Joseph, Y.; Besnard, I.; Rosenberger, M.; Guse, B.; Nothofer, H.-G.; Wessels, J. M.; Wild, U.; Knop-Gericke, A.; Su, D.; Schlögl, R.; Yasuda, A.; Vossmeyer, T. Self-Assembled Gold Nanoparticle/Alkanedithiol Films: Preparation, Electron Microscopy, XPS-Analysis, Charge Transport, and Vapor-Sensing Properties†. *The Journal of Physical Chemistry B* **2003,** *107* (30), 7406-7413.

26. Ibañez, F. J.; Zamborini, F. P. Chemiresistive Sensing with Chemically Modified Metal and Alloy Nanoparticles. *Small* **2012,** *8* (2), 174-202.

27. Geddes, L. A. Historical evolution of circuit models for the electrode-electrolyte interface. *Ann Biomed Eng* **1997,** *25* (1), 1-14.

28. Cho, E. J.; Lee, J.-W.; Ellington, A. D. Applications of Aptamers as Sensors. *Annual Review of Analytical Chemistry* **2009,** *2* (1), 241-264.

29. Song, S.; Wang, L.; Li, J.; Fan, C.; Zhao, J. Aptamer-based biosensors. *TrAC Trends in Analytical Chemistry* **2008,** *27* (2), 108-117.

30. Hagen, J. A.; Kim, S. N.; Kelley-Loughnane, N.; Naik, R. R.; Stone, M. O. Selective vapor phase sensing of small molecules using biofunctionalized field effect transistors. **2011**, 80180B-80180B.

31. Kybert, N. J.; Lerner, M. B.; Yodh, J. S.; Preti, G.; Johnson, A. T. C. Differentiation of Complex Vapor Mixtures Using Versatile DNA–Carbon Nanotube Chemical Sensor Arrays. *ACS Nano* **2013,** *7* (3), 2800-2807.

32. Lu, Y.; Goldsmith, B. R.; Kybert, N. J.; Johnson, A. T. C. DNA-decorated graphene chemical sensors. *Applied Physics Letters* **2010,** *97* (8), 083107.

33. Sinden, R. R. *DNA Structure and Function*; Academic Press1994.

34. Rothemund, P. W. K. Folding DNA to create nanoscale shapes and patterns. *Nature* **2006,** *440* (7082), 297-302.

35. Chen, Y.-S.; Hong, M.-Y.; Huang, G. S. A protein transistor made of an antibody molecule and two gold nanoparticles. *Nat Nano* **2012,** *7* (3), 197-203.

36. Nagraj, N.; Slocik, J. M.; Phillips, D. M.; Kelley-Loughnane, N.; Naik, R. R.; Potyrailo, R. A. Selective sensing of vapors of similar dielectric constants using peptide-capped gold nanoparticles on individual multivariable transducers. *Analyst* **2013,** *138* (15), 4334-4339.